NASA Technical Paper 1783

Aerothermal Environment in Chordwise Gaps Between Split Elevons at Mach 6.8

L. Roane Hunt

DECEMBER 1980

NASA

NASA Technical Paper 1783

Aerothermal Environment in Chordwise Gaps Between Split Elevons at Mach 6.8

L. Roane Hunt
Langley Research Center
Hampton, Virginia

NASA
National Aeronautics
and Space Administration

Scientific and Technical
Information Branch

1980

SUMMARY

A large-scale model that represents a wing-elevon junction on a Shuttle-type entry vehicle was aerothermally tested in the Langley 8-Foot High-Temperature Structures Tunnel. The purpose of the test was to study the flow pattern between elevons and to determine the pressure and heat load within the chordwise gaps formed by adjacent elevons and by the stub fairing which separates the elevons. Tests were performed at a free-stream Mach number of 6.8 with a turbulent boundary layer on the wing and elevon. Nominal test conditions were a dynamic pressure of 62 kPa and a total temperature of 1870 K to produce a free-stream unit Reynolds number of 4.6×10^6 m^{-1}. Both model angle of attack and elevon deflection angle were varied from 0 to 15°, and gap widths between the stub and elevons were varied from 0 to 1.19 cm. The corresponding variation in gap width between elevons was from 7.26 to 9.65 cm.

Test results indicate that heating in the narrow gaps between the stub and elevons (near the elevon hinge point) occurs primarily along the aft edge of the stub near the windward surface of the wing. Elevon-stub gap heating is proportional to wing heating and is independent of elevon deflection. Gap pressure and heating are inversely proportional to gap width. Maximum measured heating was 36 percent of the turbulent heating on the wing and occurred for an elevon-stub gap width of 0.18 cm.

The aerodynamic heating within the larger gap between the elevons (downstream of the hinge point) is proportional to the heating on the windward surfaces of the elevons except near the leeward surface. Gap heating varies inversely with gap width. Maximum heating of 30 percent of the turbulent heating on the elevon was obtained with an elevon gap width of about 7.7 cm. The heating within the large gaps between elevons and the narrow gap adjacent to the stub is only slightly affected by the Reynolds number variation of the present tests.

INTRODUCTION

Winged hypersonic vehicles, such as the Space Shuttle, require wing-elevon control surfaces that can tolerate the high aerothermal loads of hypersonic flight. The Space Shuttle incorporates split elevons on each wing as described in reference 1. Thus far, primary emphasis has been given to determining the heat load within the cove between the wing and elevon (refs. 2 and 3). The split elevons are separated by a stub which serves as a structural fairing and an end seal for the cove. Originally, the stub was designed with narrow chordwise gaps between it and each elevon, and the heating within these gaps was of great concern.

Since the complex flow between elevons is not amenable to an analytical solution and there had not been any published studies of gap heating for this configuration, a limited experimental study was made of the aerodynamic heating

between elevons for the Space Shuttle. The Shuttle design criterion was defined on the basis of unpublished data from a small-scale model tested in an arc tunnel which indicated that elevon sidewall heating could be assumed equal to the heating to the elevon windward surface. More recent unpublished results from a 0.04-scale model tested in the same facility with laminar flow indicated even greater heating in this area. However, reliable detailed heating distributions are difficult to obtain from such small-scale tests.

A large-scale model that represents a Shuttle-type wing-elevon junction where adjacent elevons are separated by a stub fairing was aerothermally tested in the Langley 8-Foot High-Temperature Structures Tunnel. The purpose of the test was to study the flow pattern between elevons and to determine the pressure and heat load within the chordwise gaps formed by the elevons and stub and by the adjacent elevons. Tests were performed at a free-stream Mach number of 6.8 with a turbulent boundary layer on the wing and elevon. Nominal test conditions were a dynamic pressure of 62 kPa and a total temperature of 1870 K to produce a free-stream unit Reynolds number of 4.6×10^6 m^{-1}. Tests were also performed at a reduced temperature of 1500 K and at reduced unit Reynolds numbers to 1.05×10^{-6} m^{-1}. Both the model angle of attack and elevon deflection angle were varied from 0 to 15°, and gap widths between the stub and elevons were varied from 0 to 1.19 cm. The corresponding variation in gap width between elevons was from 7.26 to 9.65 cm. This paper presents results of these large-scale tests.

SYMBOLS

d	normal distance into gap from windward surface (fig. 6(a)), m
p	pressure, Pa
q	dynamic pressure, Pa
$\dot{q}$	heating rate, W/m^2
r	radial distance from wing trailing edge (fig. 6(a)), m
R	unit Reynolds number, m^{-1}
T	temperature, K
W	gap width between elevons, m
w	gap width between elevon and stub, m
x,y,z	model coordinates (fig. 6(a)), m
α	angle of attack, deg
δ	elevon deflection angle, deg

Subscripts:

e	elevon surface
ℓ	lower elevon
t	total
u	upper elevon
w	wing surface
∞	free stream

APPARATUS AND TESTS

Model

A wing-elevon model shown in figure 1 was aerothermally tested in the Langley 8-Foot High-Temperature Structures Tunnel. The model consisted of a flat wedge with a sharp leading edge, a circular leeward surface, and two elevon flaps separated by a stub. Fences were attached to each side of the model to ensure two-dimensional flow on the wing portion of the model. Near the leading edge, flow trips that were sized and spaced in accordance with reference 4 were attached to the model to produce an even turbulent boundary layer on the windward surface. The model, fabricated with 1.27-cm-thick steel walls, was mounted vertically on a wedge-shaped center support about which the model could rotate for angles of attack from 0 to 15°. The two elevons were hinged in the stub and the upper and lower fences and could be rotated independently from 0 to 15°. Elevon position was fixed before each test by bolting the elevons to the fences. On the basis of stub width, the elevons were approximately 50 percent shorter than those designed for the Space Shuttle.

Photographs of the model installed in the wind tunnel are presented in figure 2. Figures 2(a) and (b) are front and side views, and in figure 2(c), the upper elevon has been removed to show the stub. Pertinent model dimensions are given in figure 3 which is an exploded view of the model. The model was 246.0 cm long and 132.0 cm wide. Maximum model depth was 30.5 cm. The length from the leading edge to the elevon hinge line was 200.0 cm. The elevons were 45.7 cm long, 62.2 cm wide at the leading edge, and 61.0 cm wide at the trailing edge. Stub width was 4.9 cm.

The elevon-wing junction was sealed to eliminate flow in the cove area formed by the elevons and wing. The gaps between the stub and elevons and the larger gap between the two elevons were not sealed. Spanwise seals were used in conjunction with the model fences to form a closed cavity between the wing hinge section and the elevon as shown in figure 4. Although the open side of the cavity is exposed to the stub forward of the hinge, the seals restrict any possible flow through the junction. However, there was a narrow spanwise gap at the junction outside of the closed cavity as shown in figure 4. High pres-

sure at the wing-elevon junction could produce spanwise flow, as illustrated in figure 5, that would reach the stub and contribute to the flow in the elevon-stub gaps.

The model instrumentation locations, the model coordinate system, and the distances r and d are illustrated in figure 6. The wing trailing edge, which is the origin of the radial distance r, is located by x and z coordinates of -3.43 and -7.62 cm, respectively. The locations of the pressure orifices and thermocouples on the model wing and elevon windward surfaces are indicated in figure 6(a). In figure 6(b), the instrument distribution, on the stub sidewalls is indicated. Although the primary objective of these tests was to determine the aerothermal load to the sidewall of the stub, the elevon sidewalls were also instrumented. The instrument distribution on the sidewall of the elevons is indicated in figure 6(c). Table I presents the exact coordinates of instrumentation for which data are tabulated in this paper. Photographs in figure 7 of the stub alone and attached to the model show the thermocouple-instrumented thin plates that were mounted flush with the model surface. Details of the plate are presented in figure 8. A chromel-alumel thermocouple was attached to a 0.08-cm-thick stainless steel plate, which was held in position with two screws. The plates were insulated from the model by a cork material to minimize thermal conduction between the plate and the model structure. Computations indicate that conduction errors in heating-rate measurements are negligible for the present tests.

Facility

The model was tested in the Langley 8-Foot High-Temperature Structures Tunnel. This facility is a hypersonic blowdown wind tunnel that uses the combustion products of methane and air as the test medium and operates at a nominal Mach number of 6.8, at total combustor pressures between 3.4 and 24.1 MPa, and at total temperatures between 1400 and 2000 K. Corresponding free-stream Reynolds numbers are between 1×10^6 and 10×10^6 m^{-1}. These conditions simulate the aerothermal flight environment at Mach 6.8 in the altitude range between 25 and 40 km. The model is retained below the test chamber during tunnel startup and shutdown and is inserted when the desired stream conditions are established. Additional information pertaining to this facility may be found in reference 4.

Tests

The model was tested at the conditions listed in table II which include the tunnel dynamic pressure, total temperature, free-stream unit Reynolds number, model angle of attack, elevon deflection angle, and gap widths. The model was tested primarily at a dynamic pressure of 62 kPa and a total temperature of 1870 K to produce a free-stream unit Reynolds number of 4.6×10^6 m^{-1}. The model angle of attack, elevon deflection, and gap widths were varied to parametrically study their effects on the pressure and heating within the gaps.

The initial test, indicated in table II, was conducted with the spanwise gap, described earlier, sealed at the ends with silicone rubber adhesive to prevent any spanwise flow and thereby isolate the effect of spanwise flow on gap heating.

For the maximum gap width, model angle of attack (α) and elevon deflection angle (δ) were varied from 0 to 15°. Nominal conditions of $\alpha = 10°$ and $\delta = 10°$ were chosen for comparison purposes when other test parameters such as gap width were varied. The gaps were varied by placing various thickness shims between the elevons and the fences. The gaps between the stub and elevons (w) were varied from 0 to 1.19 cm; the corresponding variation in the larger gap between the two elevons (W) was from 7.26 to 9.65 cm. The model was also tested with unsymmetric elevon-stub gaps by fixing the lower elevon at $w_\ell = 0.18$ cm and adjusting the upper elevon for w_u values of 1.23 and 0.59 cm. With $w_u = 0.59$ cm and $w_\ell = 0.18$ cm, α and δ were varied as in the previous tests with the maximum gap width. The model was also tested with unsymmetric elevon deflections. The lower elevon deflection was fixed at 10° while the upper elevon deflection was varied from 0 to 15°.

Additional tests were made at off-nominal tunnel flow conditions. One test was made at a reduced temperature of 1500 K and two other tests were made at reduced dynamic pressures of 45.1 and 14.9 kPa for unit Reynolds numbers of 3.22×10^6 and 1.05×10^6 m^{-1}.

RESULTS AND DISCUSSION

Oil-Flow Visualization

The windward flow on the model near the elevon-stub region is described by the typical oil-flow pattern shown in figure 9. This pattern was obtained during the test with maximum gap width and with α and δ at 10°. The pattern indicates that the flow is straight on the wing and elevon except near the edges of the gaps. The waviness of the oil streaks on the lower elevon is caused by machine irregularities during fabrication.

The gap flow is described by the oil-flow patterns on the sidewalls of the stub and lower elevon (upper elevon removed) shown in figure 10. These patterns were obtained with the elevon deflected 10° and the model angle of attack varied from 0 to 15°. The flow around the stub sidewall and base is insignificant. However, the oil pattern on the elevon downstream of the stub indicated that the flow between the elevons is significant and varies appreciably with angle of attack. At $\alpha = 0°$ (fig. 10(a)), the oil flowed toward the center of the elevon sidewall from both the windward and leeward sides of the model, and although a separation was not clearly indicated, the flow appeared to reattach near the center. As α was increased, the flow pattern changed so that the oil flowed predominately from the windward side of the model for $\alpha = 15°$.

Wing and Elevon Surface Pressures and Heating Rates

Measured surface pressures on the wing and elevon are compared with predictions in figure 11 for the various test conditions. The data fall along the 45° line representing agreement. Pressures were predicted from surveys of tunnel test media reported in reference 4, the flow properties of the combustion-product test medium from reference 5, and the oblique shock relationships from reference 6.

Measured heating rates on the windward surfaces of the wing and elevon are compared with turbulent predictions in figure 12 for the various test conditions. Predicted heating rates were obtained using Eckert's reference enthalpy method described in reference 7 for a turbulent boundary layer. The model leading edge was used as the virtual origin since the flow was tripped near the leading edge. The same virtual origin was used for both the wing and the elevon with the respective predicted local pressures. The measured heating rates on the wing were about 20 percent below the predictions; this result is consistent with measured flat-plate heating rates in the same facility presented in reference 4.

In this report, measured pressures and heating rates within the gaps are referenced to the wing and elevon pressures and heating rates (measurement locations shown in fig. 6(a)) that are listed in table III for each test. Normalized pressures and heating rates for pertinent locations on the stub base, both sidewalls of the stub, and the sidewall of each elevon are presented in tables IV and V. These normalized heating rates with a turbulent reference cannot be compared directly with the unpublished data obtained with a laminar reference, because the heating rates in separated flow regions are not totally dependent upon the boundary layer condition of the attached flow.

Elevon-Stub Gap Pressures and Heating Rates

Flow penetration into the narrow gaps between the elevons and stub was not extensive as indicated by oil-flow patterns and aerodynamic heating rates measured on the gap walls. Typical gap heating rates, normalized by the reference wing heating rate, are plotted in figure 13 as a function of radial distance from the wing trailing edge. Data obtained on the stub sidewalls adjacent to the upper and lower elevons are represented by unticked and ticked symbols, respectively. Results are presented for elevon-stub gap widths of 1.19, 0.59, and 0.18 cm, for an elevon deflection of 10°, and for wing angles of attack of 0, 5°, 10°, and 15°. Most of the heating occurred along the aft edge of the stub. The peak heating occurred at the corner of the stub sidewall nearest the windward surface of the wing. The peak heating ratio ($\dot{q}/\dot{q}_w$) was about 0.27 for the large gap width and about 0.36 for the small width. The gap heating appears to be a logarithmic function of r. As α was increased, heating to the gap interior increased, probably because of greater flow through the gap.

The effect of elevon deflection angle on elevon-stub gap heating is shown in figure 14. Normalized gap heating is plotted against radial distance from the wing trailing edge for gap widths of 1.19, 0.59, and 0.18 cm and an angle of attack of 10°. Gap heating is directly related to the heating level on the wing

ahead of the gap and independent of elevon deflection between 0 and 15°. The oil-flow patterns and heating results indicate that the flow probably enters the elevon-stub gaps from the wing surface and not from the elevon surface. Therefore, the effect of elevon deflection can be neglected when determining gap heating near the hinge line of the elevon.

The effect of elevon-stub gap width on gap pressure and heating is shown in figures 15 and 16. Gap pressure normalized by wing pressure is plotted against gap width in figure 15 for two locations along the aft edge of the stub sidewall. Model angle of attack and elevon deflection angle are 10°. Gap pressure varies inversely with gap width. As gap width is reduced, the gap pressure nearest the windward surface approaches the pressure on the wing surface.

Gap heating varies with gap width in a similar manner, as shown in figure 16. Elevon-stub gap heating nearest the windward surface varies inversely with gap width as did the gap pressure. However, heating to the gap interior decreased with reduced gap width because the flow through the gap is probably reduced so that a greater portion of the flow energy is transferred to the gap entrance and less energy remains to penetrate into the interior. This trend was seen in aerothermal studies of spanwise cove heating (refs. 3 and 8) where leakage was reduced and the flow energy was absorbed near the entrance for short exposures. Therefore, the heating distribution should vary with time and greater heating to the gap interior should occur as the gap entrance reaches equilibrium temperature. The gap heating for the tests with unequal gap widths on each side of the stub (unsymmetric elevon-stub gaps, table II) showed the same relationship with gap width as that shown in figure 16. Therefore, the elevon-stub gap heating was not affected by the size of the gap on the opposite side of the stub, so that heating results from the gaps on either side of the stub can be evaluated independently.

The effect on elevon-stub gap pressure and heating of the local Reynolds number on the wing surface is shown in figures 17 and 18. Gap pressure normalized by wing pressure is plotted against unit Reynolds number for two locations along the aft edge of the stub. The pressure ratio is independent of Reynolds number near the windward surface, but increases on the interior as Reynolds number is decreased. As Reynolds number is increased, the pressure difference through the gap is also increased. This difference indicates potential for greater flow and hence increased heating with increasing Reynolds number, as shown in figure 18. Although the heating near the windward surface of the stub is closer to the wing heating for the lower Reynolds numbers, the actual heat flux and the overall heat load increased with Reynolds number. This trend is similar to that noticed in figure 16 where higher heating near the wing surface resulted in less heating to the interior because of a decrease in gap flow rate.

Elevon Gap Pressures and Heating Rates

The flow through the large gap between the elevons produced higher convective heating and some localized flow impingement areas (as indicated by the oil-flow patterns in fig. 10) where peak heating probably occurred. However, insufficient instrumentation was located on the elevon sidewalls to accurately define

these peak heating areas. Limited elevon gap heating distributions normal to the elevon windward surface were obtained and typical results are presented in figure 19 for various elevon deflection angles up to 15°. Results are presented for an angle of attack of 10° and gap widths of 9.65 and 8.08 cm. These results are for locations 40.6 cm from the elevon hinge point. The unticked and ticked data symbols represent the results on the sidewalls of the upper and lower elevons, respectively.

In figure 19, elevon gap heating rates are normalized by the reference heating rates on the windward surfaces of the elevons (fig. 6(a)). Heating results for the three locations on the windward half of the surface are directly related to windward surface heating and appear to be independent of elevon deflection. However, heating results on the leeward half of the surface varied inversely with δ, indicating interference from the flow off the leeward surface of the model. Gap heating appears to peak just beyond a depth of 5 cm, and the peak value decreased with increased gap width. Peak heating values of $\dot{q}/\dot{q}_e = 0.16$ and 0.28 occurred for elevon gap widths of 9.65 and 8.08 cm, respectively. Lower heating nearest the windward edge of the elevon probably occurred because of flow separation produced as the flow from the windward surface expanded around the corner and turned into the gap. The oil-flow pattern along the edge (fig. 10) supports the idea that flow separation occurred along the edge. These normalized peak heating ratios obtained with a turbulent boundary layer are much less than the Space Shuttle design criterion of 1.0 derived with a laminar boundary layer on both the wing and elevons as described earlier. The difference is probably due to the change in the reference heating from turbulent to laminar, but the absolute values of heating inside the gap are probably not that different.

In the test with unsymmetric elevon deflection angles, the sidewall heating on each elevon was the same function of its own elevon reference heating value $\dot{q}_e$ as that shown in figure 19. Generally, sidewall heating was not affected by deflection angle of the adjacent elevon for the range of angles tested. Therefore, no appreciable mixing of the flow in the gaps occurred near the elevon sidewalls and the flow along the elevon sidewalls would be characteristic of external boundary layer flow or developing flow between parallel plates.

Similar elevon gap heating results are presented in figure 20 for various model angles of attack and $\delta = 10°$. Again, the peak heating occurred at a depth of about 5 cm. In this comparison, the greatest influence of leeward flow occurred at $\alpha = 5°$. Influence of leeward flow on elevon sidewall heating is dependent on both α (windward flow conditions) and δ (pressure differential across elevon), as indicated by a comparison of the results presented in figures 19 and 20.

The flow effects produced by varying elevon gap width are difficult to define since they are localized and the instrumentation was sparse. The gap pressure for two locations are plotted against gap width in figure 21. The gap was varied from 7.26 to 9.65 cm. The angle of attack and elevon deflection angle were 10°. The pressure levels at the two orifices, located at d = 15.2 cm, differ greatly, but the pressure does not vary with gap width, again indicating that the flow is characteristic of boundary layer flow. As shown in figure 22, elevon gap heating near the windward surface of the elevon

varies significantly with gap width even though the heating at $d = 15.2$ cm is independent of W (similar to pressure). The value of $\dot{q}/\dot{q}_e$ peaks at 0.3 at $d = 5.2$ cm for a gap width of about 7.7 cm. Apparently, the flow impingement shifts as the aspect ratio of the gap varies. A general definition of aspect ratio for this application could be the ratio of the length from the hinge point to the gap width. Insufficient data exist to substantiate the exact location of the flow impingement.

Normalized elevon gap heating varies only slightly with local unit Reynolds number on the wing surface, as shown in figure 23. Some of the variations could be caused by small changes in flow direction as it expands around the elevon gap edges. The most significant change occurred near the leeward surface of the wing. The trends are very similar to those noted for the elevon-stub gap.

CONCLUDING REMARKS

A large-scale model that represents a wing-elevon junction on a Shuttle-type entry vehicle was aerothermally tested in the Langley 8-Foot High-Temperature Structures Tunnel. The purpose of the test was to study the flow pattern between elevons and to determine the pressure and heat load within the chordwise gaps formed by adjacent elevons and by the stub fairing which separates the elevons. Tests were performed at a free-stream Mach number of 6.8 with a turbulent boundary layer on the wing and elevon. Nominal test conditions were a dynamic pressure of 62 kPa and a total temperature of 1870 K to produce a free-stream unit Reynolds number of 4.6×10^6 m^{-1}. Tests were also performed at a reduced temperature of 1500 K and at reduced unit Reynolds numbers to 1.05×10^6 m^{-1}. Both model angle of attack and elevon deflection angle were varied from 0 to 15^o, and gap widths between the stub and elevons were varied from 0 to 1.19 cm. The corresponding variation in gap width between elevons was from 7.26 to 9.65 cm.

Test results indicate that heating in the narrow gaps between the stub and elevons (near the elevon hinge point) occurs primarily along the aft edge of the stub near the windward surface of the wing. Elevon-stub gap heating is proportional to wing heating and is independent of the elevon deflection angle. Gap pressure and heating are inversely proportional to gap width. The maximum measured heating was 36 percent of the turbulent heating on the wing and occurred for an elevon-stub gap width of 0.18 cm.

The aerodynamic heating within the larger gap between elevons (downstream of the hinge point) is proportional to the heating on the windward surfaces of the elevons except near the leeward surface. The flow along the elevon sidewalls is typical of boundary layer type flow and characterized primarily by the flow on the elevon surfaces, in particular the windward side. Gap heating decreases with gap width. A peak heating of 30 percent of the turbulent heating on the elevon was obtained with an elevon gap width of about 7.7 cm. Peak heating values normalized by turbulent reference heating were much less than the Space Shuttle design criterion derived with a laminar reference. The difference was probably due to the change in reference heating from turbulent to laminar, and the absolute heating inside the gap was probably not that differ-

ent. The heating within the large gaps between elevons and the narrow gap adjacent to the stub is only slightly affected by the Reynolds number variation of the present tests.

National Aeronautics and Space Administration
Langley Research Center
Hampton, VA 23665
December 3, 1980

REFERENCES

1. Strouhal, George; and Tillian, Donald J.: Testing the Shuttle Heat-Protection Armor. Astronaut. & Aeronaut., vol. 14, no. 1, Jan. 1976, pp. 57-65.

2. Scott, C. D.; Murray, L. P.; and Milhoan, J. D.: Shuttle Elevon Cove Aerodynamic Heating by Internal Flow. AIAA Paper 77-757, June 1977.

3. Deveikis, William D.; and Bartlett, Whitney: Pressure and Heat-Transfer Distributions in a Simulated Wing-Elevon Cove With Variable Leakage at a Free-Stream Mach Number of 6.9. NASA TM-74095, 1978.

4. Deveikis, William D.; and Hunt, L. Roane: Loading and Heating of a Large Flat Plate at Mach 7 in the Langley 8-Foot High-Temperature Structures Tunnel. NASA TN D-7275, 1973.

5. Leyhe, E. W.; and Howell, R. R.: Calculation Procedure for Thermodynamic, Transport, and Flow Properties of the Combustion Products of a Hydrocarbon Fuel Mixture Burned in Air With Results for Ethylene-Air and Methane-Air Mixtures. NASA TN D-914, 1962.

6. Ames Research Staff: Equations, Tables, and Charts for Compressible Flow. NACA Rep. 1135, 1953. (Supersedes NACA TN-1428.)

7. Kays, W. M.: Convective Heat and Mass Transfer. McGraw-Hill Book Co., Inc., c.1966.

8. Hunt, L. Roane: Aerothermal Analysis of a Wing-Elevon Cove With Variable Leakage. NASA TP-1703, 1980.

TABLE I.- LOCATION OF PRESSURE AND HEATING-RATE INSTRUMENTATION ON MODEL

(a) Pressure orifices

Orifice	x, cm	y, cm	z, cm	r, cm	d, cm
External surfaces					
p_w	-1.55	0	-7.62		0
$p_{e,u}$	41.33	33.55	-7.62		0
$p_{e,\ell}$	41.33	-33.55	-7.62		0
Stub base					
p_6	2.79	0	-5.28		2.34
p_7	10.11	0	5.13		12.75
Stub upper sidewall					
p_{11}	1.24	2.44	-5.28	5.26	2.34
p_{13}	8.79	2.44	5.46	17.88	13.08
p_{16}	-2.64	2.44	-6.35	1.45	1.27
p_{17}	-5.08	2.44	-5.41	2.87	2.21
Stub lower sidewall					
p_{31}	1.19	-2.44	-5.23	5.31	2.39
p_{33}	8.81	-2.44	5.46	17.96	13.08
p_{36}	2.69	-2.44	-6.40	1.47	1.22
p_{37}	5.11	-2.44	-5.33	2.77	2.29
Upper elevon surface					
p_{59}	2.54	2.44	7.62		15.24
p_{60}	15.88	3.71	7.62		15.24
p_{61}	30.48	3.71	7.62		15.24
Lower elevon surface					
p_{79}	2.54	-2.44	7.62		15.24
p_{80}	15.80	-3.71	7.62		15.24
p_{81}	33.02	-3.71	7.62		15.24

TABLE I.- Continued

(b) Thermocouples

Thermocouples	x, cm	y, cm	z, cm	d, cm	r, cm
External Surfaces					
$\dot{q}_w$	-7.90	0	-7.62	0	
$\dot{q}_{e,u}$	21.01	33.55	-7.62	0	
$\dot{q}_{e,\ell}$	21.01	-33.55	-7.62	0	
Stub base					
$\dot{q}_6$	1.90	0	-6.55	1.07	
$\dot{q}_7$	7.04	0	.74	8.36	
$\dot{q}_8$	12.88	0	9.09	16.71	
Stub upper sidewall					
$\dot{q}_{11}$	0.51	2.44	-6.27	1.35	4.11
$\dot{q}_{12}$	2.77	2.44	-3.02	4.60	7.67
$\dot{q}_{13}$	5.82	2.44	1.19	8.81	12.73
$\dot{q}_{14}$	11.86	2.44	9.78	17.40	23.09
$\dot{q}_{15}$	-4.09	2.44	-6.35	1.27	1.52
$\dot{q}_{16}$	-1.09	2.44	-4.19	3.43	4.11
$\dot{q}_{17}$	-3.58	2.44	-3.30	4.32	4.32
Stub lower sidewall					
$\dot{q}_{31}$	0.41	-2.44	-6.40	1.22	4.09
$\dot{q}_{32}$	2.69	-2.44	-3.10	4.52	7.70
$\dot{q}_{33}$	5.89	-2.44	1.22	8.84	12.75
$\dot{q}_{34}$	11.89	-2.44	9.68	17.30	23.04
$\dot{q}_{35}$	-4.14	-2.44	-6.30	1.32	1.47
$\dot{q}_{36}$	-1.19	-2.44	-4.29	3.33	4.09
$\dot{q}_{37}$	-3.61	-2.44	-3.30	4.32	4.32

TABLE I.- Concluded

(b) Concluded

Thermocouples	x, cm	y, cm	z, cm	d, cm	r, cm
Upper elevon sidewall					
$\dot{q}_{51}$	0.10	2.44	-5.08	2.54	
$\dot{q}_{52}$	3.81	2.44	-5.08	2.54	
$\dot{q}_{53}$	20.35	3.71	-5.08	2.54	
$\dot{q}_{54}$	40.64	3.71	-5.00	2.62	
$\dot{q}_{55}$	3.84	2.44	-2.54	5.08	
$\dot{q}_{56}$	20.32	3.71	-2.52	5.10	
$\dot{q}_{57}$	40.64	3.71	-2.46	5.10	
$\dot{q}_{60}$	19.99	3.71	7.57	15.19	
$\dot{q}_{61}$	40.34	3.71	7.52	15.14	
$\dot{q}_{62}$	39.37	3.71	20.07	27.69	
Lower elevon sidewall					
$\dot{q}_{71}$	0	-2.44	-5.08	2.54	
$\dot{q}_{72}$	3.86	-2.44	-5.08	2.54	
$\dot{q}_{73}$	20.29	-3.71	-5.08	2.54	
$\dot{q}_{74}$	40.67	-3.71	-5.11	2.51	
$\dot{q}_{75}$	3.84	-2.44	-2.54	5.08	
$\dot{q}_{76}$	20.32	-3.71	-2.54	5.08	
$\dot{q}_{77}$	40.67	-3.71	-2.57	5.05	
$\dot{q}_{80}$	19.76	-3.71	7.34	14.96	
$\dot{q}_{81}$	39.98	-3.71	7.39	15.01	
$\dot{q}_{82}$	39.37	-3.71	20.19	27.81	

TABLE II.- TEST CONDITIONS

Test	q_∞, kPa	$T_{t,\infty}$, K	R_∞, m^{-1}	α, deg	δ_u, deg	δ_ℓ, deg	w_u, cm	w_ℓ, cm	W, cm
Sealed spanwise gap									
1	61.9	1890	4.56×10^6	10	10	10	1.19	1.19	9.65
Maximum elevon-stub gaps									
2	62.6	1790	4.82×10^6	0	0	0	1.19	1.19	9.65
3	62.8	1830	4.72	0	10	10	1.19	1.19	9.65
4	62.4	1890	4.59	10	0	0	1.19	1.19	9.65
5	61.3	1870	4.56	10	5	5	1.19	1.19	9.65
6	61.7	1870	4.59	10	10	10	1.19	1.19	9.65
7	62.6	1930	4.53	10	15	15	1.19	1.19	9.65
8	62.2	1830	4.69	15	10	10	1.19	1.19	9.65
9	61.8	1830	4.66	5	10	10	1.19	1.19	9.65
Reduced elevon-stub gaps									
10	62.7	1820	4.76×10^6	10	10	10	0.55	0.57	8.51
11	62.4	1920	4.53	10	10	10	.27	.32	7.92
12	62.1	1960	4.43	10	10	10	.12	.18	7.57
13	62.6	1900	4.56	10	10	10	0	0	7.26
Unsymmetric elevon-stub gaps									
14	63.1	1900	4.63×10^6	10	10	10	1.23	0.18	8.66
15	62.4	1960	4.46	10	10	10	.59	.18	8.08
16	62.6	1910	4.56	10	0	0	.59	.18	8.08
17	62.5	1910	4.56	10	15	15	.59	.18	8.08
18	62.6	1860	4.66	5	10	10	.59	.18	8.08
19	62.3	1900	4.56	15	10	10	.59	.18	8.08
Unsymmetric elevon deflections									
20	62.6	1850	4.66×10^6	10	0	10	1.19	1.19	9.65
21	61.3	1870	4.53	10	5	10	1.19	1.19	9.65
22	62.3	1910	4.56	10	15	10	1.19	1.19	9.65
Reduced total temperature									
23	53.8	1500	4.56×10^6	10	10	10	1.19	1.19	9.65
Reduced unit Reynolds number									
24	45.1	1940	3.22×10^6	10	10	10	1.19	1.19	9.65
25	14.9	1960	1.05	10	10	10	1.19	1.19	9.65

TABLE III.- REFERENCE PRESSURES AND HEATING RATES ON WING AND ELEVON WINDWARD SURFACES

Test	p_w, kPa	$\dot{q}_w$, kW/m^2	$p_{e,u}$, kPa	$p_{e,\ell}$, kPa	$\dot{q}_{e,u}$, kW/m^2	$\dot{q}_{e,\ell}$, kW/m^2
Sealed spanwise gap						
1	8.14	183.5	26.34	27.03	611.1	624.8
Maximum elevon-stub gaps						
2	2.33	65.0	2.41	2.51	78.3	81.0
3	2.34	65.8	8.69	8.62	235.3	233.7
4	8.41	190.7	8.07	8.27	219.0	223.8
5	8.20	189.5	14.76	15.51	366.5	382.5
6	8.27	185.0	27.58	27.24	620.9	614.2
7	8.55	195.5	44.13	44.96	934.1	949.0
8	14.00	272.0	37.92	38.96	793.5	811.9
9	4.62	116.0	16.69	16.82	418.9	421.8
Reduced elevon-stub gaps						
10	8.20	175.6	27.58	27.99	618.3	626.1
11	8.20	186.1	26.55	27.10	625.3	636.3
12	8.14	199.1	26.06	26.96	654.3	673.3
13	8.07	195.7	26.55	27.72	631.2	654.8
Unsymmetric elevon-stub gaps						
14	8.07	186.9	26.20	27.79	625.2	657.2
15	8.27	206.0	26.89	27.58	665.2	679.6
16	8.00	192.5	8.07	8.27	230.6	235.6
17	8.00	182.4	42.40	43.78	954.3	980.7
18	4.65	117.6	16.20	16.41	413.9	418.3
19	13.65	289.1	36.54	38.06	815.5	844.2
Unsymmetric elevon deflection						
20	8.00	191.6	7.93	27.58	221.3	638.4
21	8.14	189.1	14.89	27.30	372.2	623.2
22	8.07	176.8	42.75	27.37	944.6	646.7
Reduced total temperature						
23	7.38	136.6	24.27	24.20	425.0	424.0
Reduced unit Reynolds number						
24	6.07	154.8	19.24	19.79	494.5	506.5
25	2.00	60.4	6.27	6.27	201.6	201.6

TABLE IV.- EXPERMENTAL PRESSURES IN MODEL GAPS

Test	Stub base		Stub upper sidewall				Stub lower sidewall				Upper elevon sidewall			Lower elevon sidewall		
	P_6/P_w	P_7/P_w	P_{11}/P_w	P_{13}/P_w	P_{16}/P_w	P_{17}/P_w	P_{31}/P_w	P_{33}/P_w	P_{36}/P_w	P_{37}/P_w	P_{59}/P_w	P_{60}/P_w	P_{61}/P_w	P_{79}/P_w	P_{80}/P_w	P_{81}/P_w
	Sealed spanwise gaps															
1	0.016	0.014	0.067	0.004	0.042	0.206	0.053	0.015	0.033	0.132	0.019	0.014	0.035	0.011	0.015	0.061
	Maximum elevon-stub gaps															
2	0.106	0.098	0.139	0.080	0.213	0.225	0.127	0.101	0.183	0.246	0.142	0.112	0.266	0.104	0.092	0.325
3	.091	.086	.097	.050	.139	.177	.080	.083	.153	.224	.094	.097	.171	.062	.094	.271
4	.017	.021	.051	.013	.164	.172	.059	.022	.115	.139	.031	.025	.057	.022	.018	.058
5	.021	.017	.049	.003	.150	.185	.058	.013	.118	.182	.028	.022	.059	.013	.018	.061
6	.050	.014	.053	.001	.107	.134	.062	.013	.111	.162	.017	.017	.040	.017	.017	.078
7	.037	.020	.060	.010	.129	.156	.071	.026	.134	.172	.031	.030	.089	.034	.026	.133
8	.019	.017	.059	.008	.102	.143	.067	.017	.099	.143	.009	.044	.089	.019	.007	.103
9	.030	.027	.052	.018	.116	.140	.055	.027	.109	.149	.033	.027	.090	.015	.024	.082
	Reduced elevon-stub gaps															
10	0.026	0.012	0.102	0.008	0.093	0.207	0.090	0.018	0.090	0.192	0.027	0.017	0.071	0.026	0.013	0.071
11	.018	.013	.162	.024	.178	.261	.162	.034	.155	.195	.046	.018	.046	.042	.013	.067
12	.012	.010	.249	.037	.271	.318	.263	.052	.237	.250	.076	.019	.062	.093	.017	.068
13	.014	.015	---	---	.521	.479	---	---	.675	.479	---	.017	.060	---	.012	.063
	Unsymmetric elevon-stub gaps															
14	0.018	0.010	0.053	0	0.105	0.135	0.291	0.052	0.238	0.244	0.015	0.015	0.056	0.096	0.018	0.074
15	.017	.013	.092	.010	.097	.204	.283	.053	.236	.242	.032	.018	.065	.098	.018	.071
16	.018	.015	.091	.012	.132	.206	.271	.052	.240	.173	.034	.019	.055	.091	.019	.046
17	.021	.012	.098	.009	.107	.238	.297	.062	.284	.305	.030	.018	.093	.110	.011	.106
18	.033	.036	.107	.019	.105	.224	.311	.061	.311	.311	.056	.033	.065	.114	.037	.081
19	.013	.008	.096	.007	.096	.210	.260	.053	.206	.240	.024	.008	.059	.088	.010	.078
	Unsymmetric elevon deflection															
20	0.020	0.016	0.055	0.003	0.160	0.220	0.060	0.019	0.103	0.129	0.020	0.021	0.038	0.016	0.023	0.051
21	.017	.015	.053	.001	.164	.160	.059	.014	.093	.130	.014	.014	.038	.010	.018	.060
22	.016	.010	.142	.005	.119	.167	.060	.013	.103	.127	.030	.021	.056	.013	.015	.071
	Reduced total temperature															
23	0.016	0.014	0.050	0	0.107	0.140	0.056	0.013	0.106	0.136	0.012	0.015	0.037	0.008	0.016	0.058
	Reduced unit Reynolds number															
24	0.022	0.014	0.056	0	0.114	0.150	0.059	0.015	0.107	0.141	0.019	0.019	0.047	0.010	0.015	0.063
25	.069	.024	.059	.010	.128	.134	.059	.031	.138	.124	.017	.017	.052	.010	.021	.076

TABLE V. - EXPERIMENTAL HEATING RATES IN MODEL GAPS

Test	Stub base			Stub upper sidewall							Stub lower sidewall						
	$\dot{q}_6/\dot{q}_w$	$\dot{q}_7/\dot{q}_w$	$\dot{q}_8/\dot{q}_w$	$\dot{q}_{11}/\dot{q}_w$	$\dot{q}_{12}/\dot{q}_w$	$\dot{q}_{13}/\dot{q}_w$	$\dot{q}_{14}/\dot{q}_w$	$\dot{q}_{15}/\dot{q}_w$	$\dot{q}_{16}/\dot{q}_w$	$\dot{q}_{17}/\dot{q}_w$	$\dot{q}_{31}/\dot{q}_w$	$\dot{q}_{32}/\dot{q}_w$	$\dot{q}_{33}/\dot{q}_w$	$\dot{q}_{34}/\dot{q}_w$	$\dot{q}_{35}/\dot{q}_w$	$\dot{q}_{36}/\dot{q}_w$	$\dot{q}_{37}/\dot{q}_w$
Sealed spanwise gap																	
1	0.0241	0.0186	0.0198	0.184	0.0359	0.0229	0.0068	0	0.0037	0.0012	0.200	0.0557	0.0309	0.0031	0	0.0043	0
Maximum elevon-stub gaps																	
2	0.0105	0.0017	-0.0035	0.236	0.0227	-0.0017	-0.0052	0.0541	0.0192	0	0.246	0.0227	0.0017	-0.0035	0.0489	0.0087	-0.0035
3	.0172	0	.0224	.269	.0207	-.0017	-.0069	.0397	.0207	.0052	.266	.0207	.0034	0	.0466	.0155	.0052
4	.0250	.2320	.0238	.242	.0476	.0137	.0048	.1050	.0071	.0030	.286	.0560	.0179	.0060	.0905	.0071	.0018
5	.0246	.0251	.0180	.288	.0563	.0156	.0035	.1070	.0090	.0084	.271	.0551	.0192	.0114	.1040	.0114	.0048
6	.0245	.0307	.0147	.262	.0595	.0288	.0123	.0982	.0184	.0092	.232	.0509	.0178	.0080	.0963	.0098	.0055
7	.0250	.0366	.0139	.258	.0600	.0215	.0058	.0888	.0075	.0070	.250	.0470	.0174	.0017	.0946	.0122	.0075
8	.0184	.0254	.0063	.282	.0572	.0442	-.0042	.1330	.0196	.0104	.277	.0730	.0225	-.0067	.1250	.0129	.0075
9	.0245	.0245	.0489	.279	.0470	.0127	.0020	.0714	.0127	.0049	.248	.0313	.0157	.0049	.0773	.0098	.0049
Reduced elevon-stub gaps																	
10	0.0226	0.0517	0.0488	0.265	0.0782	0.0220	0.0071	0.0905	0.0278	0.0187	0.254	0.0640	0.0200	0.0019	0.0911	0.0304	0.0142
11	.0262	.0488	.0140	.326	.0854	.0177	0	.0860	.0329	.0244	.305	.0652	.0211	.0006	.0720	.0335	.0207
12	.0239	.0371	.0188	.357	.0616	.0028	.0011	.0667	.0257	.0245	.340	.0473	.0040	0	.0570	.0274	.0217
13	.0145	-.0041	-.0017	0	.0017	.0012	.0023	.0133	.0012	.0017	0	.0006	.0006	.0012	.0070	.0012	.0006
Unsymmetric elevon-stub gaps																	
14	0.0249	0.0358	0.0237	0.247	0.0589	0.0267	0.0073	0.0880	0.0109	0.0049	0.349	0.0510	0.0049	0	0.0607	0.0285	0.0225
15	.0231	.0441	.0165	.258	.0628	.0165	.0044	.0650	.0231	.0154	.329	.0457	.0044	.0006	.0606	.0259	.0209
16	.0236	.0389	.0436	.242	.0495	.0153	.0035	.0696	.0195	.0100	.325	.0649	.0047	.0006	.0389	.0230	.0100
17	.0255	.0485	.0236	.261	.0572	.0193	.0044	.0846	.0236	.0156	.363	.0380	.0044	0	.0548	.0292	.0180
18	.0241	.0666	.0222	.267	.0386	.0106	0	.0473	.0203	.0125	.357	.0222	.0010	.0010	.0512	.0203	.0183
19	.0212	.0416	.0181	.243	.0726	.0243	.0055	.0664	.0196	.0141	.314	.0664	.0055	-.0020	.0550	.0294	.0220
Unsymmetric elevon deflections																	
20	0.0195	0.0231	0.0213	0.207	0.0385	0.0113	0.0036	0.0699	0.0071	0.0024	0.241	0.0456	0.0160	0.0071	0.0800	0.0024	0.0036
21	.0210	.0240	.0222	.230	.0408	.0126	.0084	.0846	.0042	.0030	.232	.0492	.0180	.0108	.0822	.0054	.0048
22	.0199	.0359	.0096	.260	.0392	.0186	0	.0706	.0013	.0032	.266	.0449	.0160	.0071	.0706	.0051	-.0077
Reduced total temperature																	
23	0.0174	0.0199	0.0174	0.203	0.0365	0.0166	0.0066	0.0673	0.0116	0.0066	0.211	0.0407	0.0133	0.0050	0.0681	0.0058	0.0033
Reduced unit Reynolds number																	
24	0.0249	0.0264	0.0117	0.269	0.0594	0.0220	0.0073	0.0799	0.0110	0.0066	0.268	0.0565	0.0198	0.0081	0.0968	0.0081	0.0037
25	.0338	.0263	.0301	.376	.0752	.0188	-.0056	.0714	.0169	.0056	.387	.0695	.0169	-.0038	.0714	.0113	0

TABLE V.- Concluded

Test	Upper elevon sidewall										Lower elevon sidewall									
	$\dot{q}_{51}/\dot{q}_w$	$\dot{q}_{52}/\dot{q}_w$	$\dot{q}_{53}/\dot{q}_w$	$\dot{q}_{54}/\dot{q}_w$	$\dot{q}_{55}/\dot{q}_w$	$\dot{q}_{56}/\dot{q}_w$	$\dot{q}_{57}/\dot{q}_w$	$\dot{q}_{60}/\dot{q}_w$	$\dot{q}_{61}/\dot{q}_w$	$\dot{q}_{62}/\dot{q}_w$	$\dot{q}_{71}/\dot{q}_w$	$\dot{q}_{72}/\dot{q}_w$	$\dot{q}_{73}/\dot{q}_w$	$\dot{q}_{74}/\dot{q}_w$	$\dot{q}_{75}/\dot{q}_w$	$\dot{q}_{76}/\dot{q}_w$	$\dot{q}_{77}/\dot{q}_w$	$\dot{q}_{80}/\dot{q}_w$	$\dot{q}_{81}/\dot{q}_w$	$\dot{q}_{82}/\dot{q}_w$
Sealed spanwise gap																				
1	0.0278	0.170	0.120	0.244	0.0674	0.450	0.395	0.0148	0.212	0.1210	0.0396	0.233	0.139	0.244	0.0705	0.463	0.458	0.0062	0.228	0.132
Maximum elevon-stub gaps																				
2	0.0925	0.194	0.014	0.108	0.0384	0	0.140	0.0873	0.483	0.0506	0.1170	0.218	0.016	0.108	0.0314	0.14	0.145	0.0750	0.508	0.073
3	.0586	.231	.155	.345	.0966	.522	.388	.1140	.345	.1280	.0603	.259	.166	.341	.0707	.514	.417	.0879	.302	.169
4	.0893	.172	.052	.070	.0786	.255	.112	.0119	.104	.1460	.1000	.174	.051	.049	.0571	.262	.119	.0117	.098	.164
5	.0820	.178	.080	.135	.0802	.322	.206	.0168	.141	.0095	.0826	.177	.081	.116	.0461	.310	.222	.0210	.146	.109
6	.0620	.184	.126	.249	.0687	.446	.406	.0215	.218	.0896	.0681	.195	.118	.215	.0503	.419	.421	.0276	.222	.149
7	.0464	.209	.172	.333	.0673	.609	.633	.0380	.362	.0696	.0534	.217	.164	.276	.0598	.600	.685	.0389	.362	.063
8	.0676	.178	.104	.175	.0768	.399	.477	.0213	.206	.0572	.0859	.181	---	.090	.0572	.301	.548	.0167	.187	.042
9	.0656	.192	.132	.302	.0763	.485	.410	.0157	.204	.3530	.0704	.212	.152	.286	.0773	.482	.443	.0186	.200	.428
Reduced elevon-stub gaps																				
10	0.0595	0.230	0.127	0.267	0.1080	0.464	0.650	0.0123	0.187	0.0659	0.0536	0.259	0.116	0.223	0.1140	0.454	0.822	0.0136	0.204	0.165
11	.0598	.192	.141	.393	.1540	.495	.967	.0122	.170	.0610	.0579	.259	.116	.279	.1440	.465	.887	.0134	.193	.116
12	.0473	.147	.126	.509	.0952	.452	.873	.0114	.166	.0792	.0490	.261	.112	.409	.1080	.431	.804	.0125	.172	.114
13	0	.040	.104	.520	0	.421	.792	.0041	.137	.1350	0	.027	.101	.524	0	.408	.756	.0046	.140	.116
Unsymmetric elevon-stub gaps																				
14	0.0686	0.192	0.141	0.313	0.0638	0.493	0.679	0.0140	0.204	0.0753	0.0510	0.267	0.112	0.188	0.1190	0.435	0.533	0.0152	0.216	0.151
15	.0479	.231	.128	.308	.1000	.455	.856	.0127	.178	.0727	.0463	.253	.112	.218	.1100	.414	.792	.0127	.183	.109
16	.0926	.140	.047	.127	.0938	.245	.284	.0094	.074	.1440	.1110	.120	.039	.086	.0849	.225	.265	.0295	.076	.198
17	.0355	.277	.195	.502	.1160	.684	1.562	.0361	.305	.0678	.0386	.355	.189	.490	.1130	.610	1.477	.0429	.279	.057
18	.0502	.258	.136	.322	.1120	.492	.583	.0154	.189	.5010	.0290	.281	.145	.269	.0560	.463	.627	.0299	.176	.483
19	.0542	.213	.106	.508	.0954	.424	.756	.0275	.164	.0459	.0550	.229	.092	.484	.1290	.393	.720	.0389	.169	.039
Unsymmetric elevon deflections																				
20	0.0782	0.147	0.052	0.090	0.0610	0.237	0.203	0.0213	0.087	0.1000	0.0610	0.185	0.116	0.209	0.0498	0.447	0.419	0.0195	0.205	0.113
21	.0678	.156	.083	.156	.0618	.327	.249	.0144	.130	.0678	.0678	.191	.124	.214	.0504	.457	.437	.0330	.231	.141
22	.0424	.218	.212	.438	.1010	.680	.752	.0302	.401	.0802	.0674	.225	.123	.220	.0507	.482	.624	.0186	.231	.122
Reduced total temperature																				
23	0.0432	0.140	0.127	0.324	0.0498	0.424	0.507	0.0266	0.208	0.1150	0.0498	0.172	0.097	0.280	0.0415	0.405	0.490	0.0282	0.211	0.124
Reduced unit Reynolds number																				
24	0.0652	0.193	0.132	0.288	0.0696	0.493	0.416	0.0154	0.224	0.0887	0.0755	0.216	0.116	0.194	0.0616	0.467	0.403	0.0169	0.232	0.111
25	.0771	.291	.156	.306	.1170	.588	.408	.0019	.182	.0282	.0940	.318	.162	.274	.1200	.551	.419	.0019	.182	.070

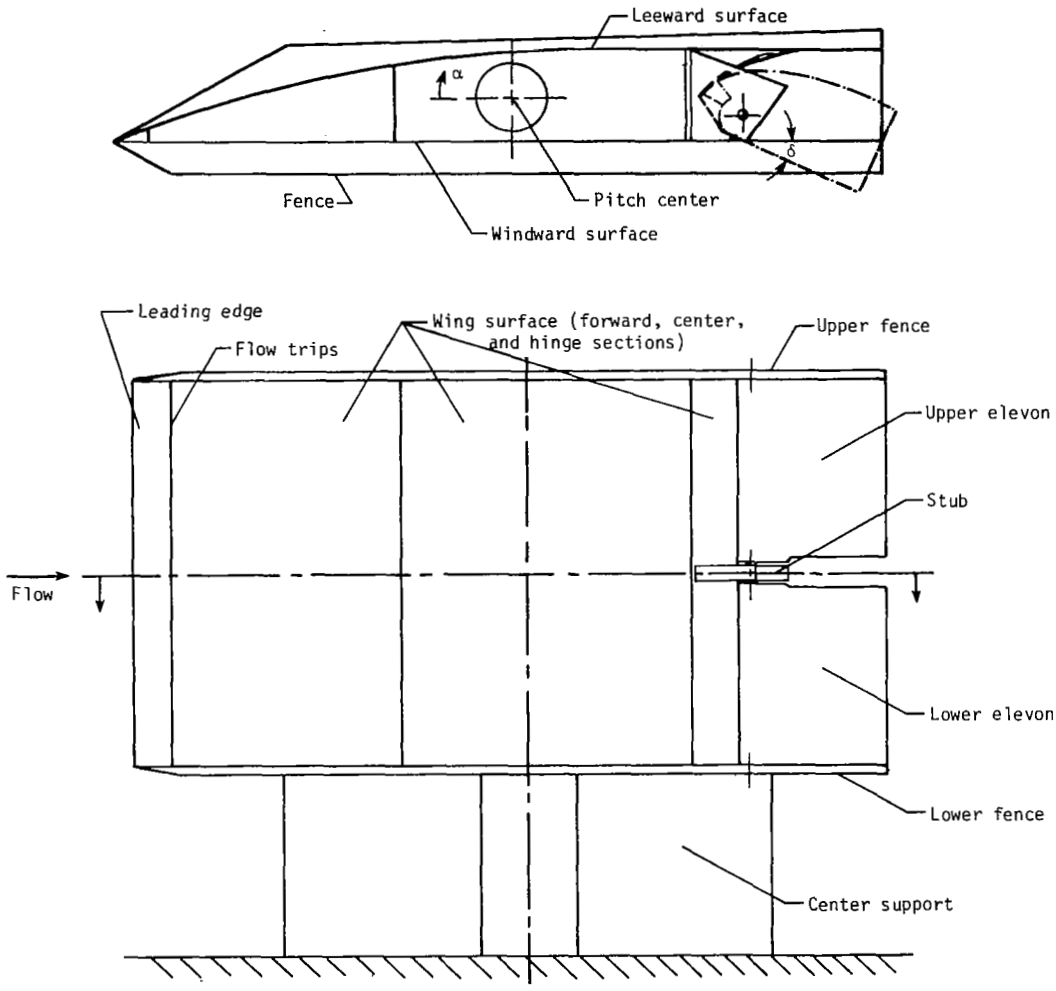

Figure 1.- Schematic of wing-elevon model.

(a) Front view. $\alpha = 10^{o}$; $\delta = 25^{o}$.

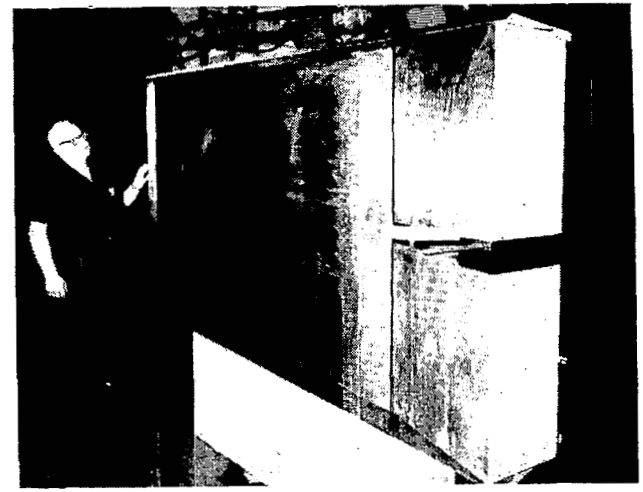

(b) Side view. $\alpha = 15^{o}$; $\delta = 15^{o}$.

(c) Side view without upper elevon. $\alpha = 15^{o}$; $\delta = 15^{o}$.

L-80-251

Figure 2.- Test model installed in Langley 8-Foot-High-Temperature Structures Tunnel.

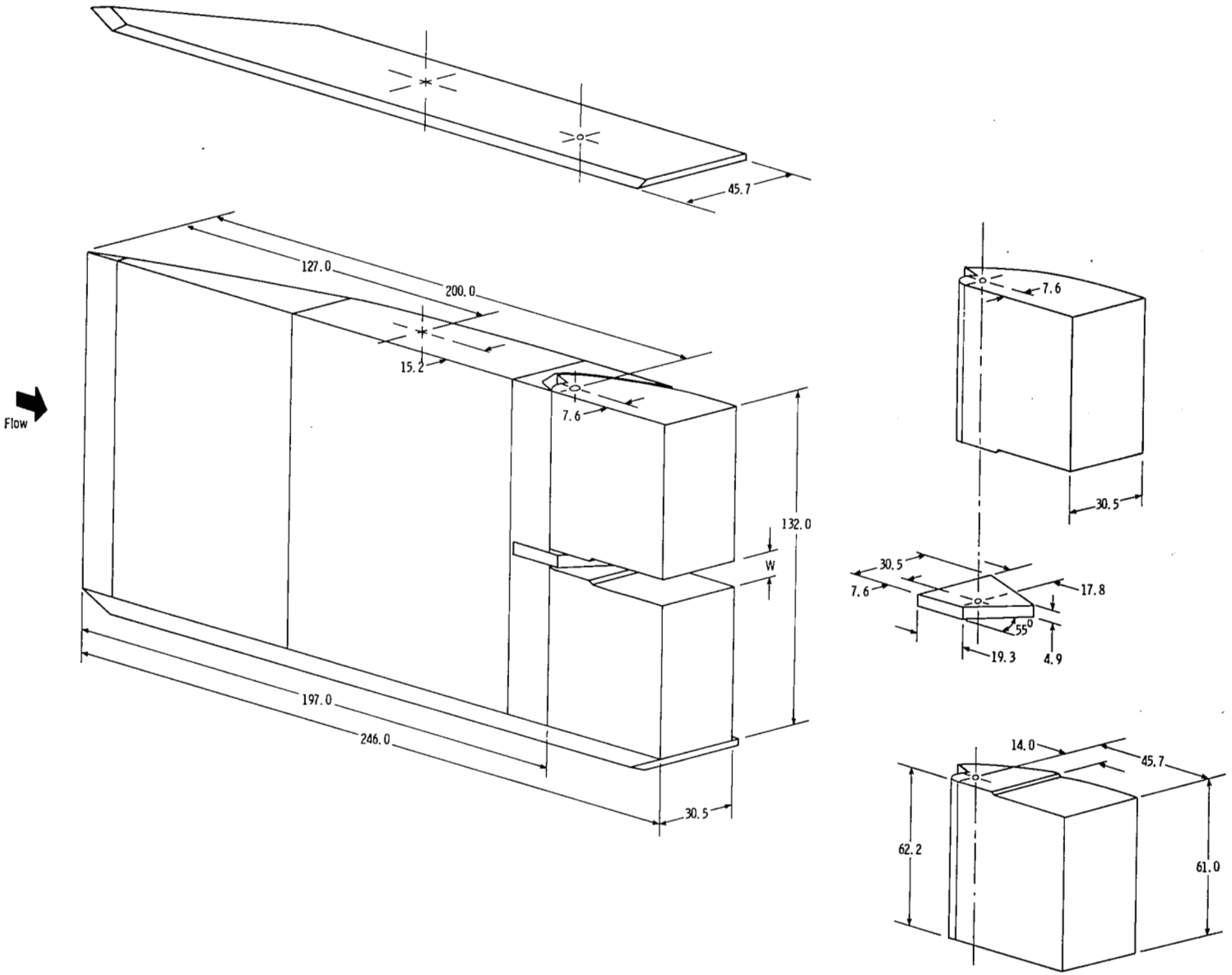

Figure 3.- Exploded view of test model. (All dimensions are in centimeters.)

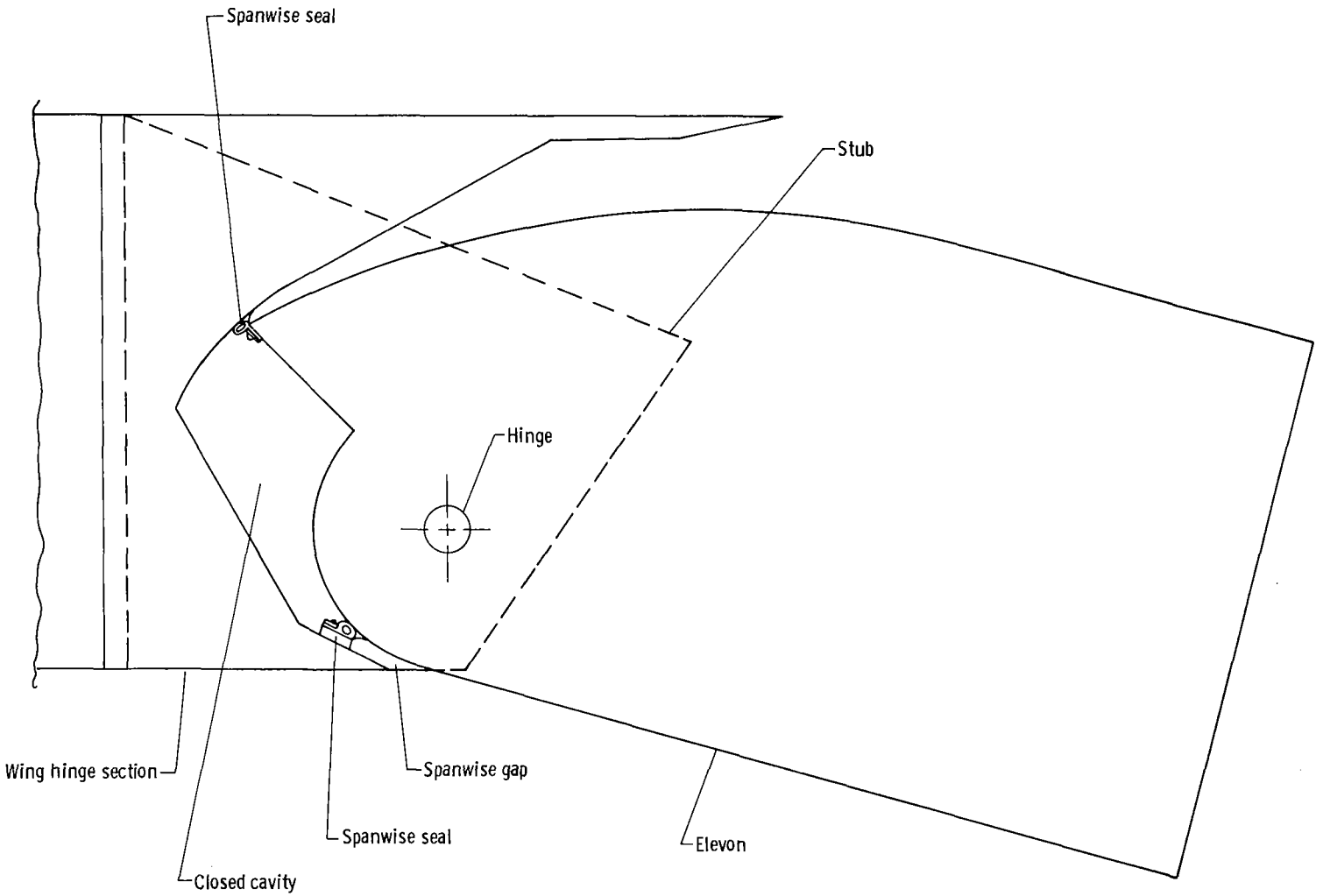

Figure 4.- Spanwise seals.

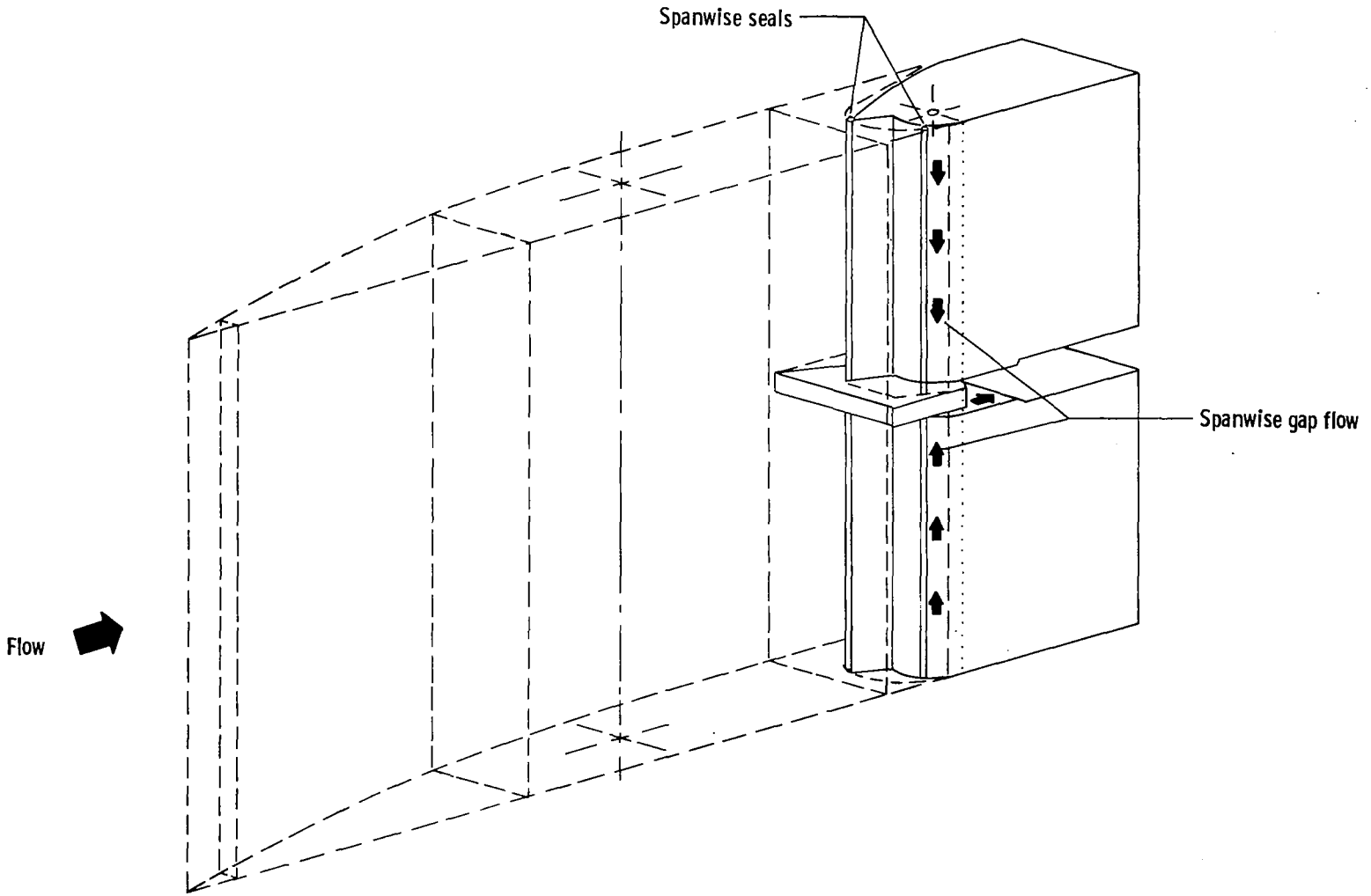

Figure 5.- Spanwise gap flow.

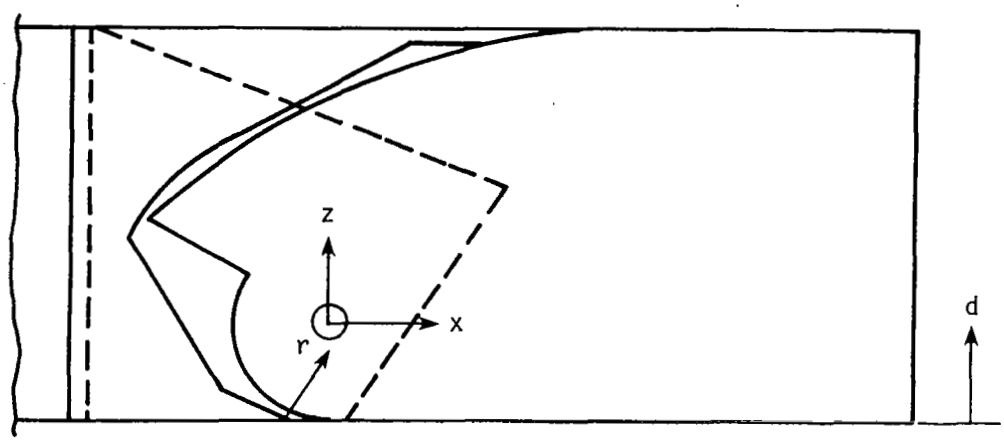

o Pressure orifice

● Heating-rate thermocouple

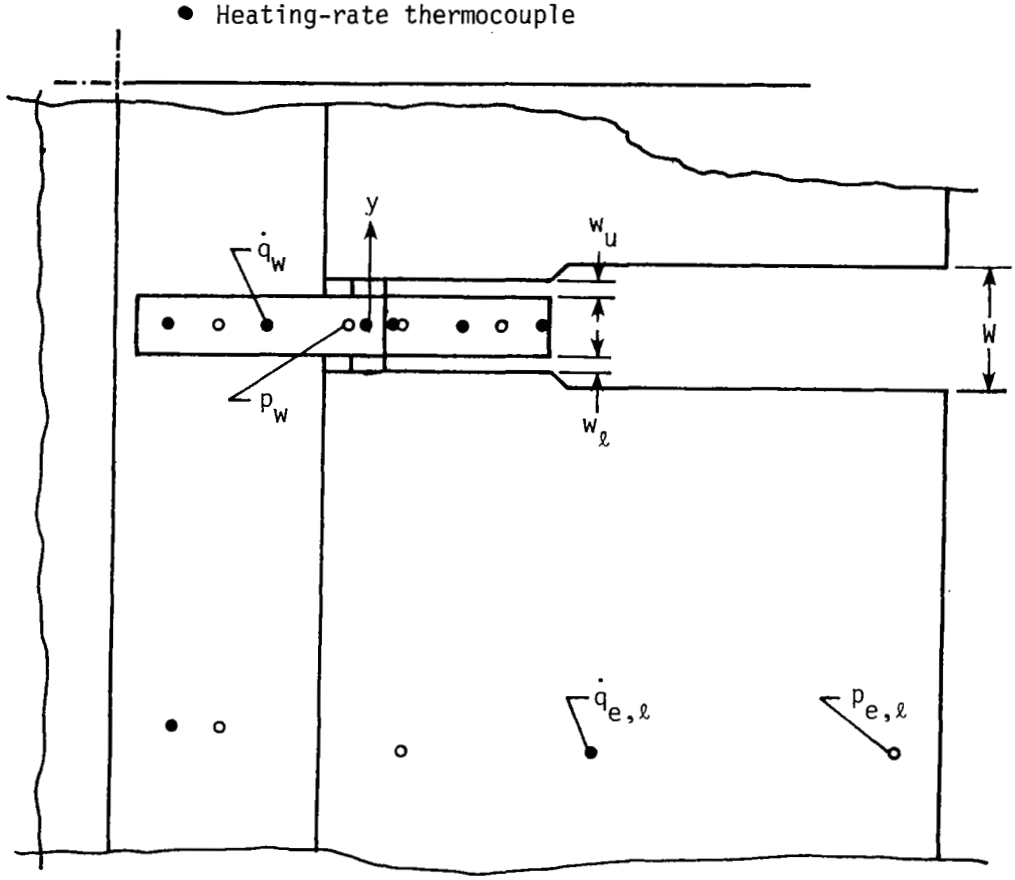

(a) Windward surfaces.

Figure 6.- Instrumentation and coordinate system.

o Pressure orifice

● Heating-rate thermocouple

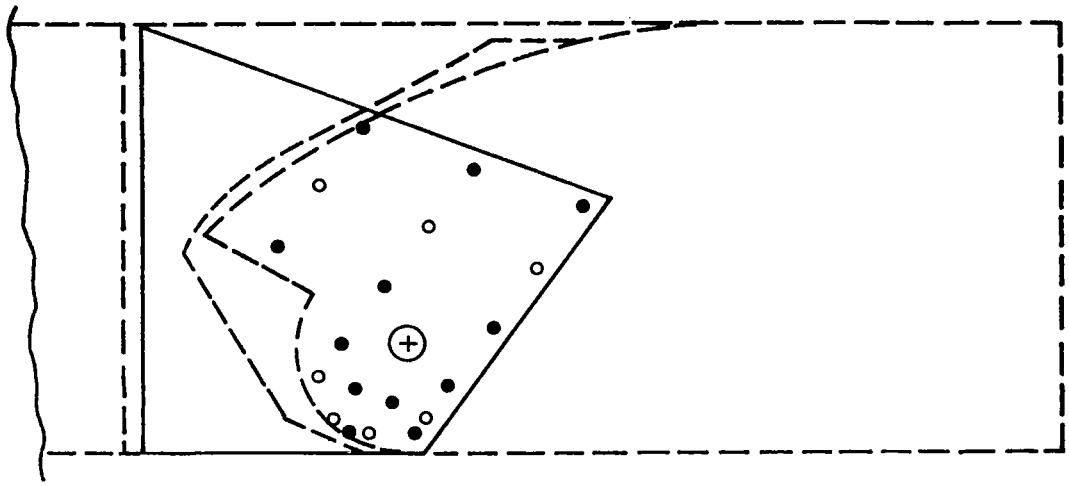

(b) Stub.

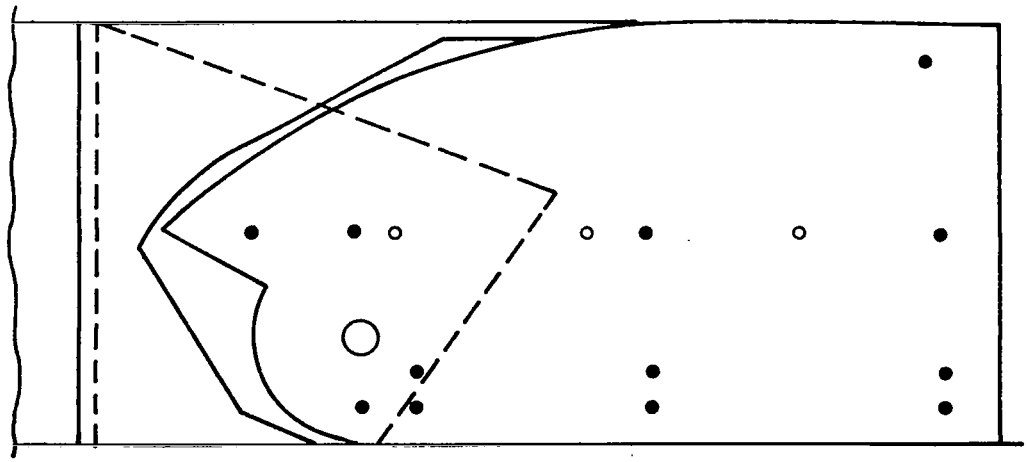

(c) Elevon.

Figure 6.- Concluded.

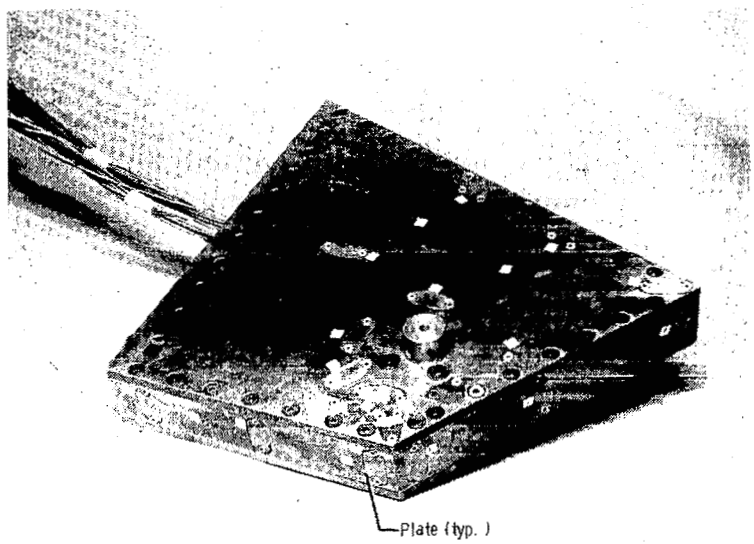

L-78-5720

(a) Stub instrumentation.

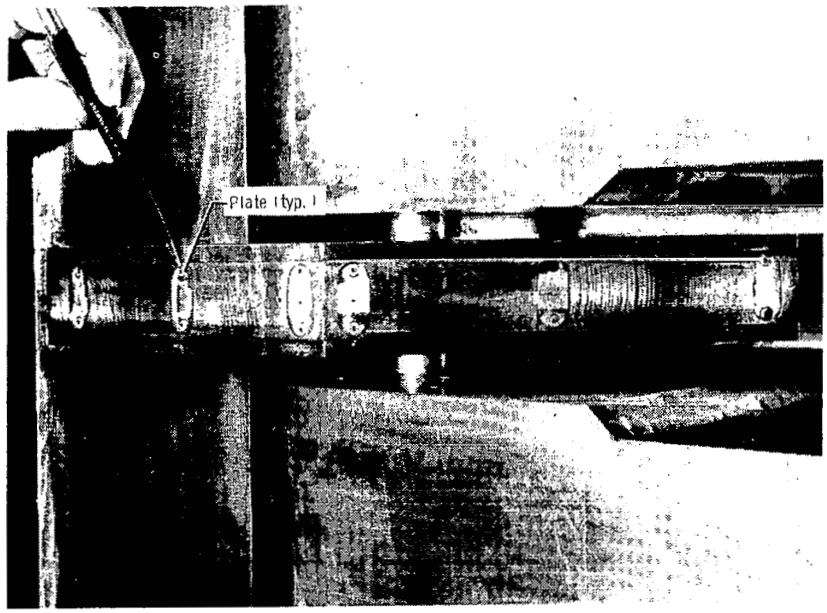

L-78-7498

(b) Stub attached to model.

Figure 7.- Heating-rate thermocouples mounted on test model surface.

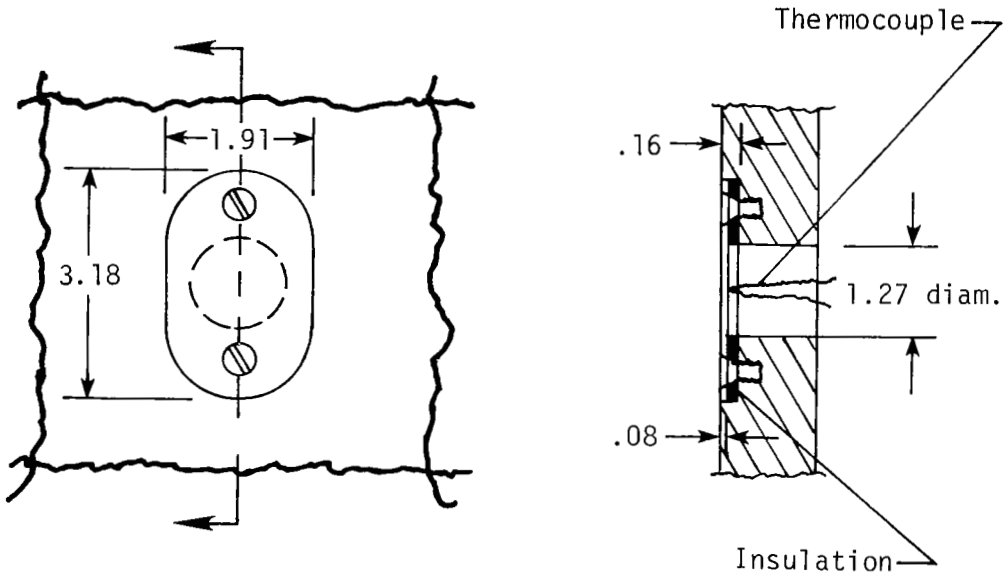

Figure 8.- Details of thermocouple-instrumented thin plate. (All dimensions are in centimeters.)

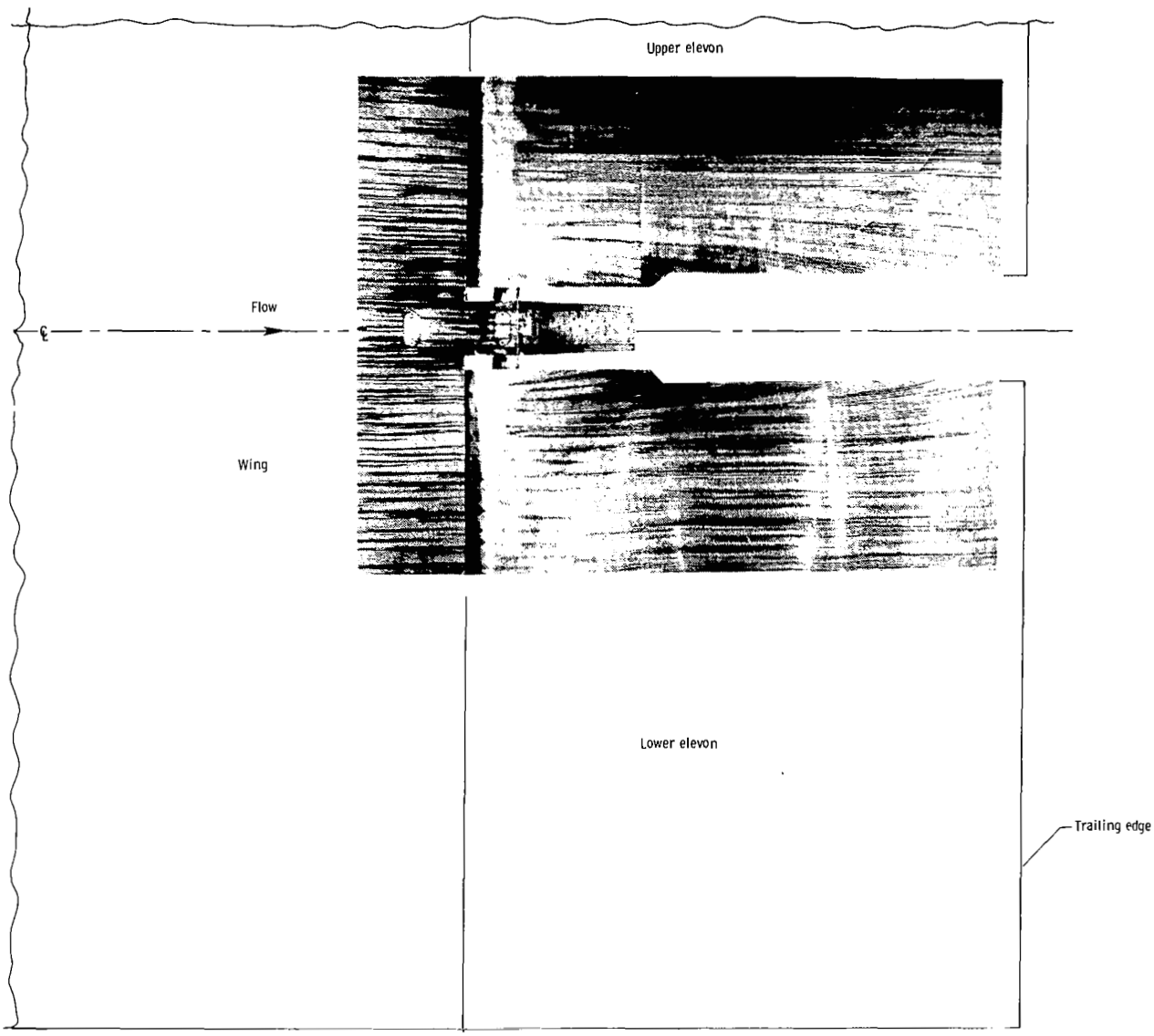

L-80-252

Figure 9.- Oil-flow pattern on wing and elevon windward surfaces. W = 9.65; $\delta = 10^{o}$; $\alpha = 10^{o}$.

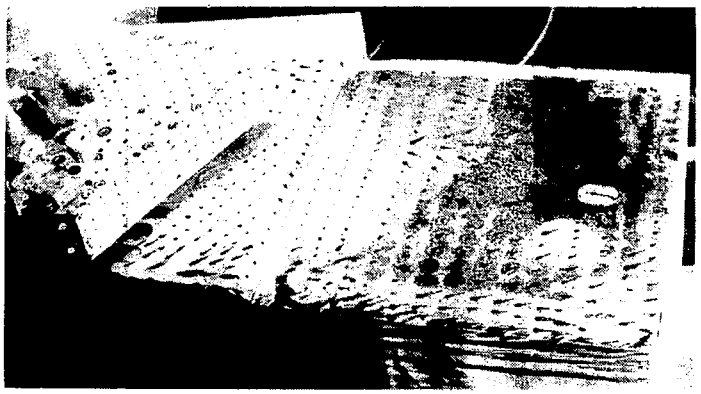

(a) $\alpha = 0.$

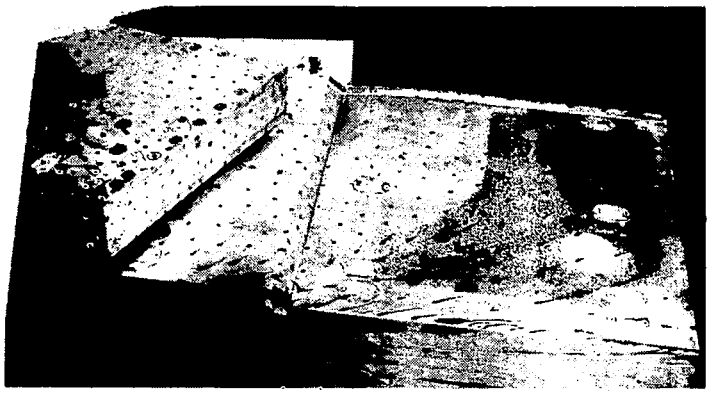

(b) $\alpha = 5^{o}.$

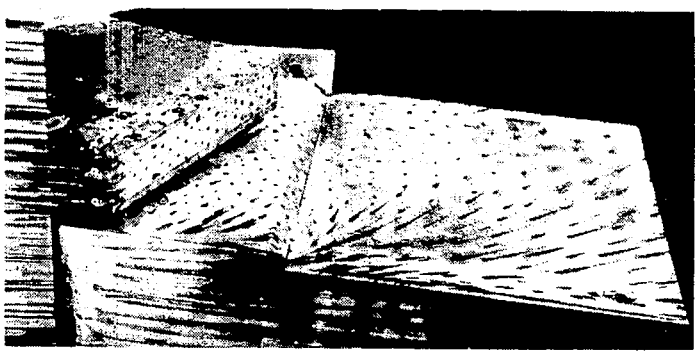

(c) $\alpha = 10^{o}.$

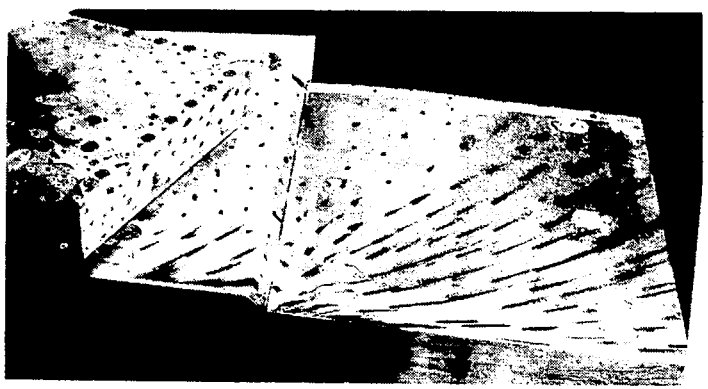

(d) $\alpha = 15^{o}.$

L-80-253

Figure 10- Oil-flow patterns on gap surfaces between elevons. $\delta = 10^{o}.$

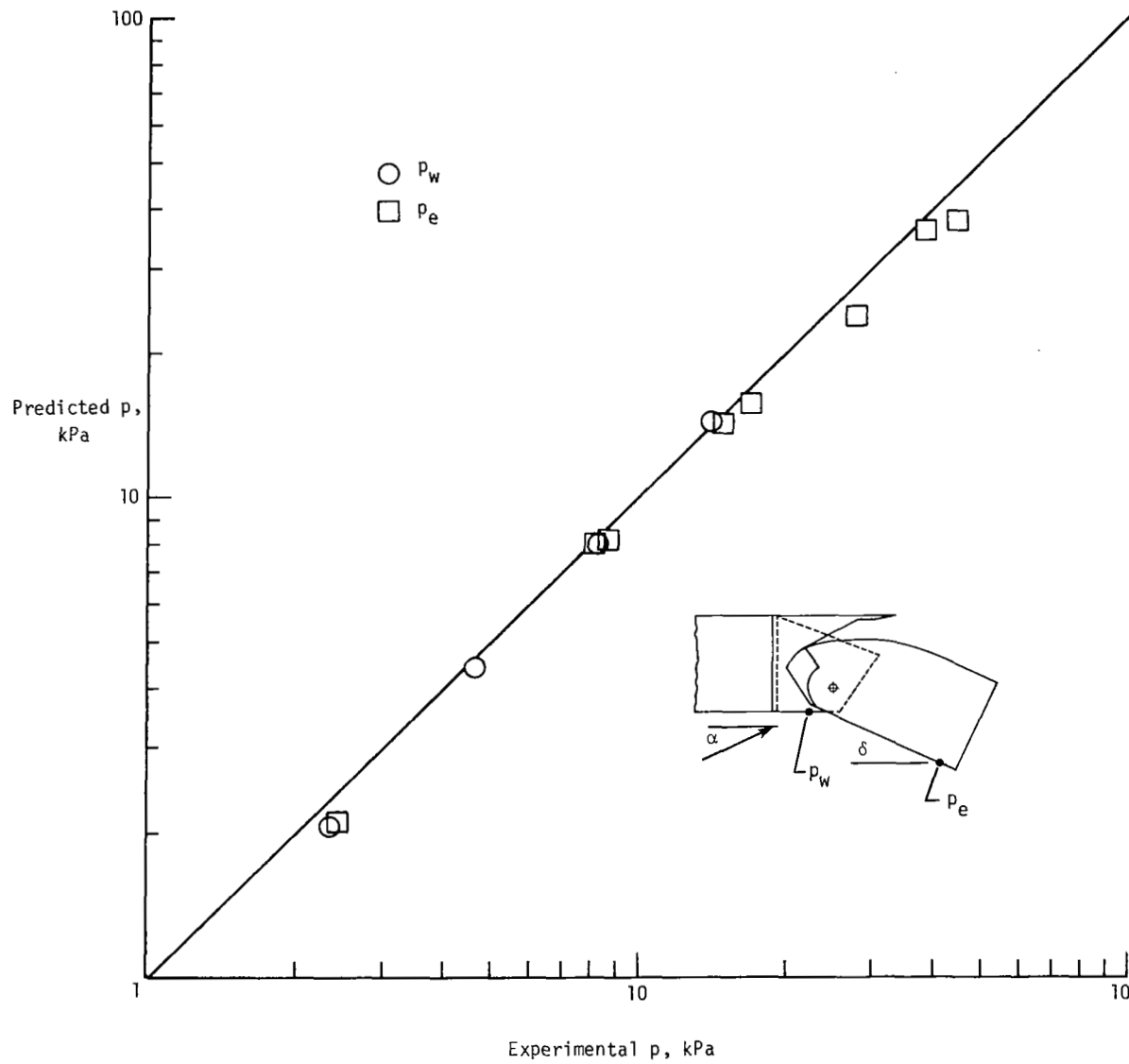

Figure 11.- Pressures on wing and elevon windward surfaces for various test conditions.

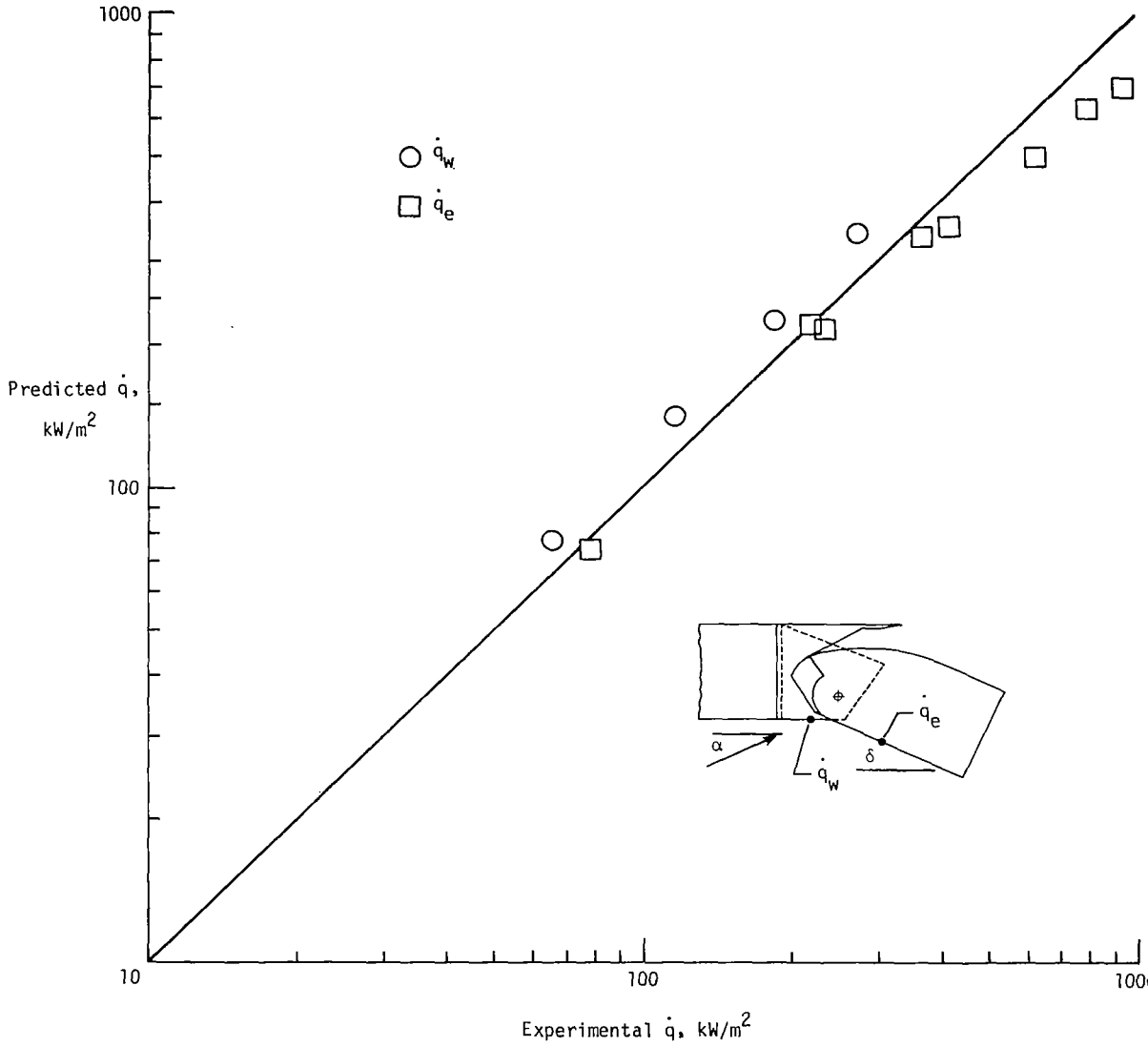

Figure 12.- Turbulent heating rates on wing and elevon windward surfaces for various test conditions.

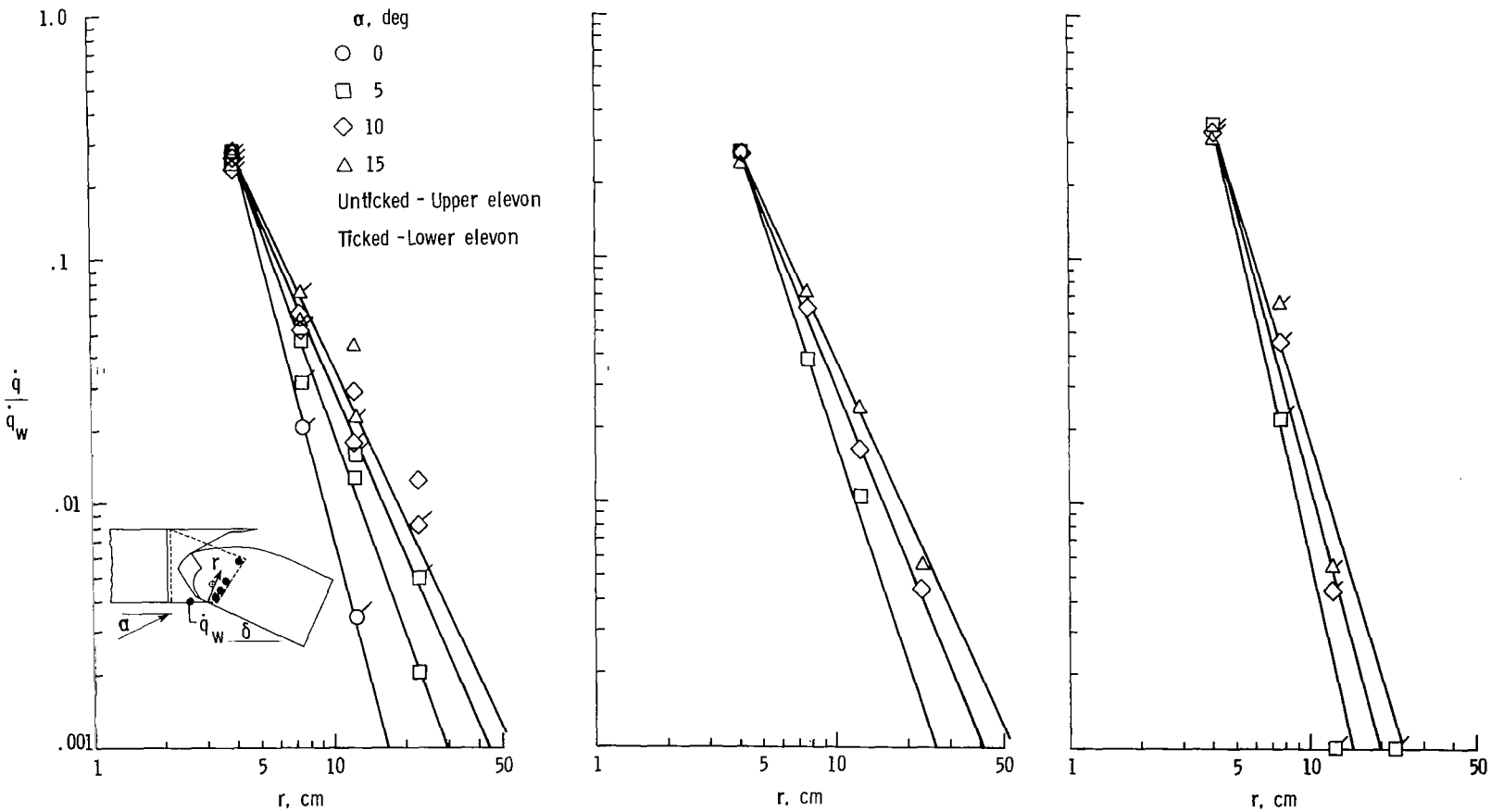

(a) w = 1.19 cm. (b) w = 0.59 cm. (c) w = 0.18 cm.

Figure 13.- Elevon-stub gap heating distribution for various angles of attack. $\delta = 10^{\circ}$.

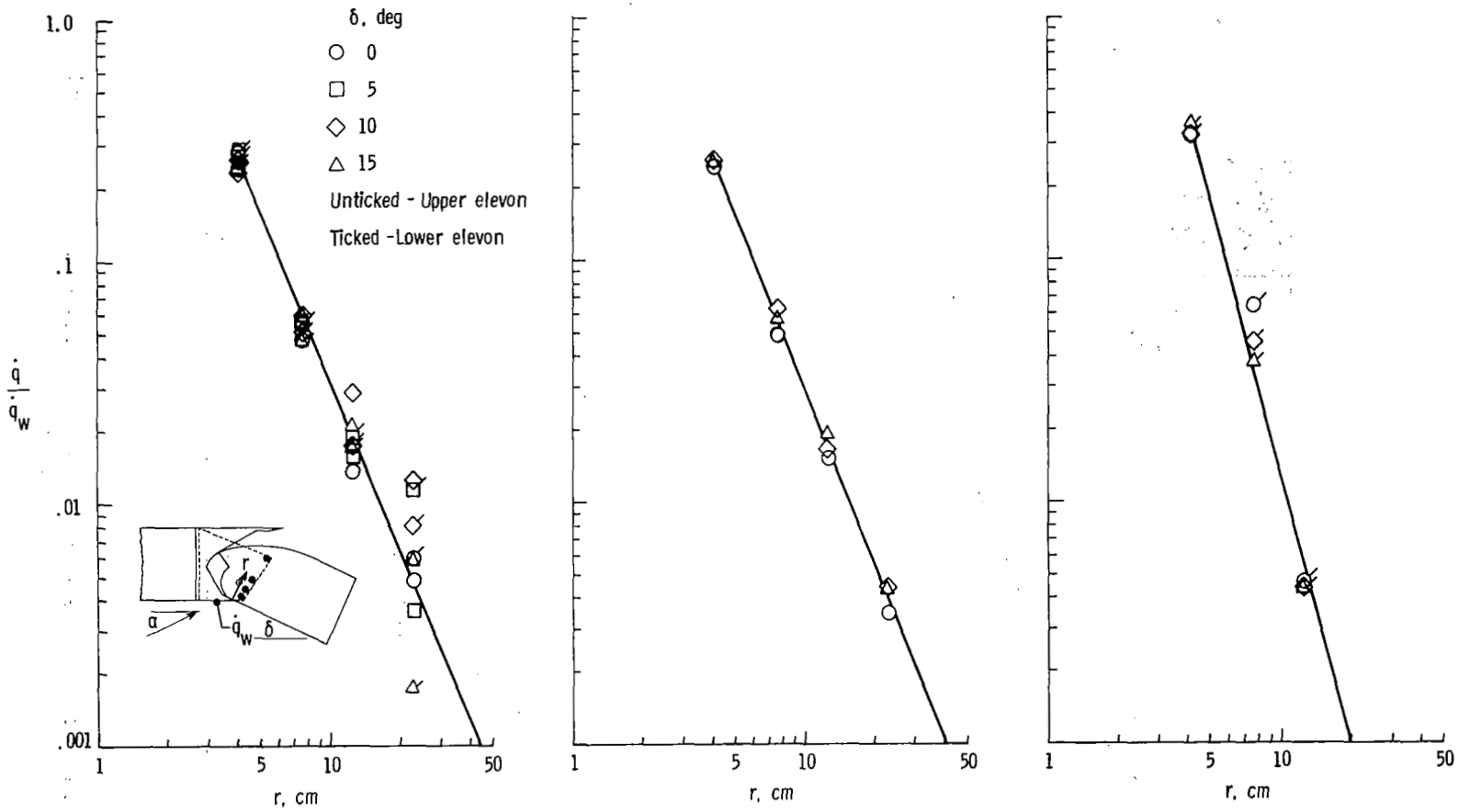

(a) w = 1.19 cm. (b) w = 0.59 cm. (c) w = 0.18 cm.

Figure 14.- Elevon-stub gap heating distribution for various elevon deflection angles. $\delta = 10^{o}$.

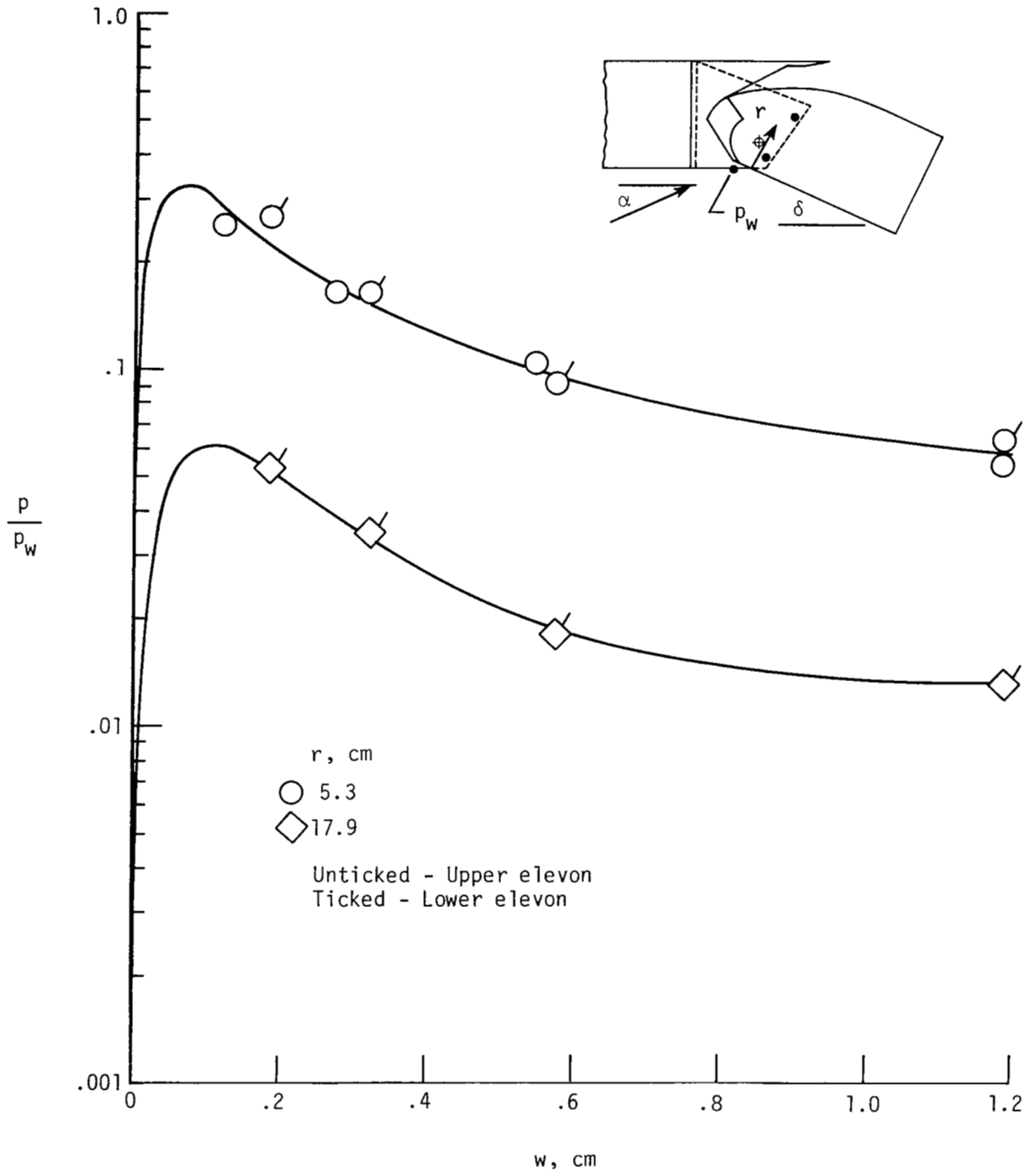

Figure 15.- Variation of elevon-stub gap pressure with gap width. $\alpha = 10^{o}$; $\delta = 10^{o}$.

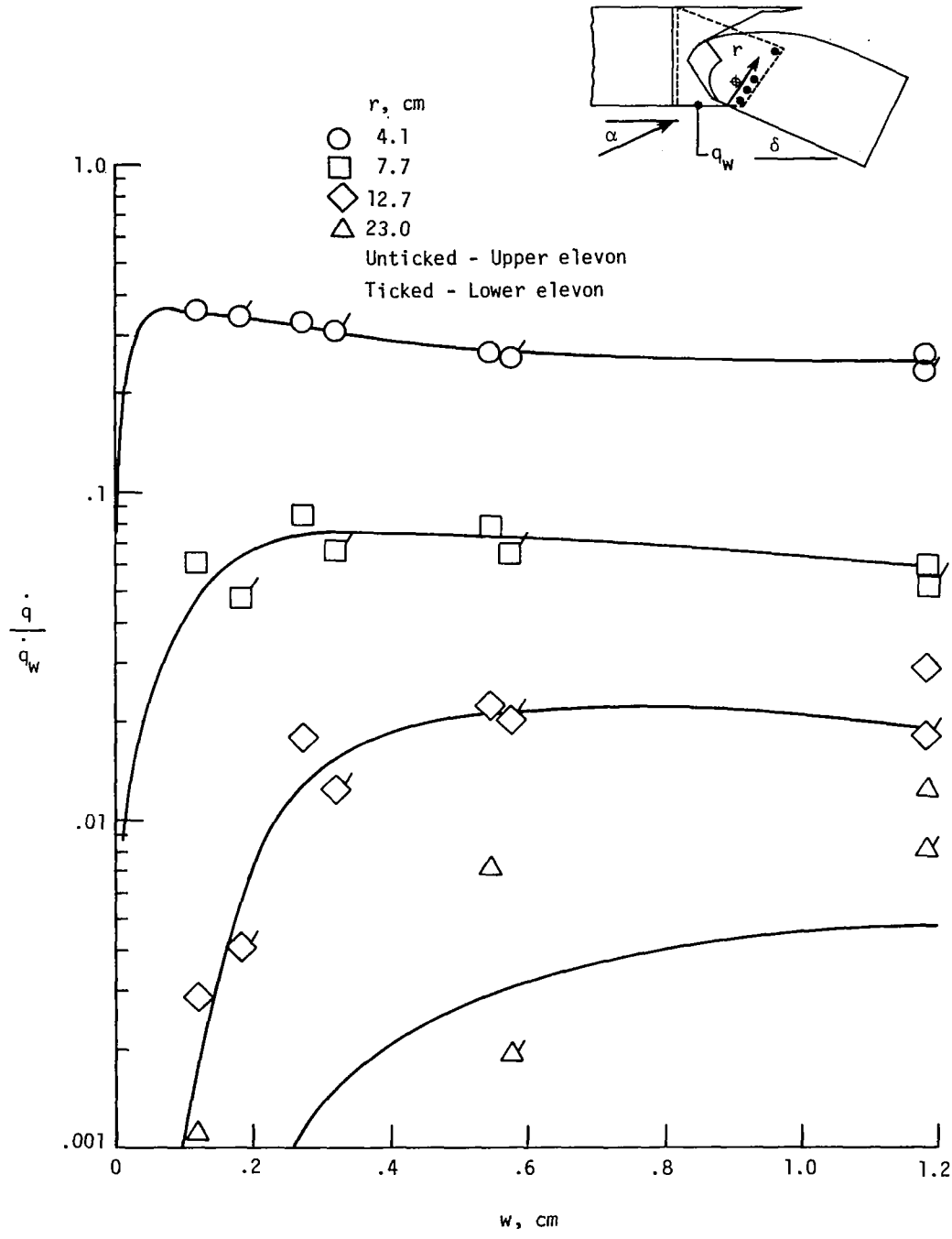

Figure 16.- Variation of elevon-stub gap heating with gap width. $\alpha = 10^{o}$; $\delta = 10^{o}$.

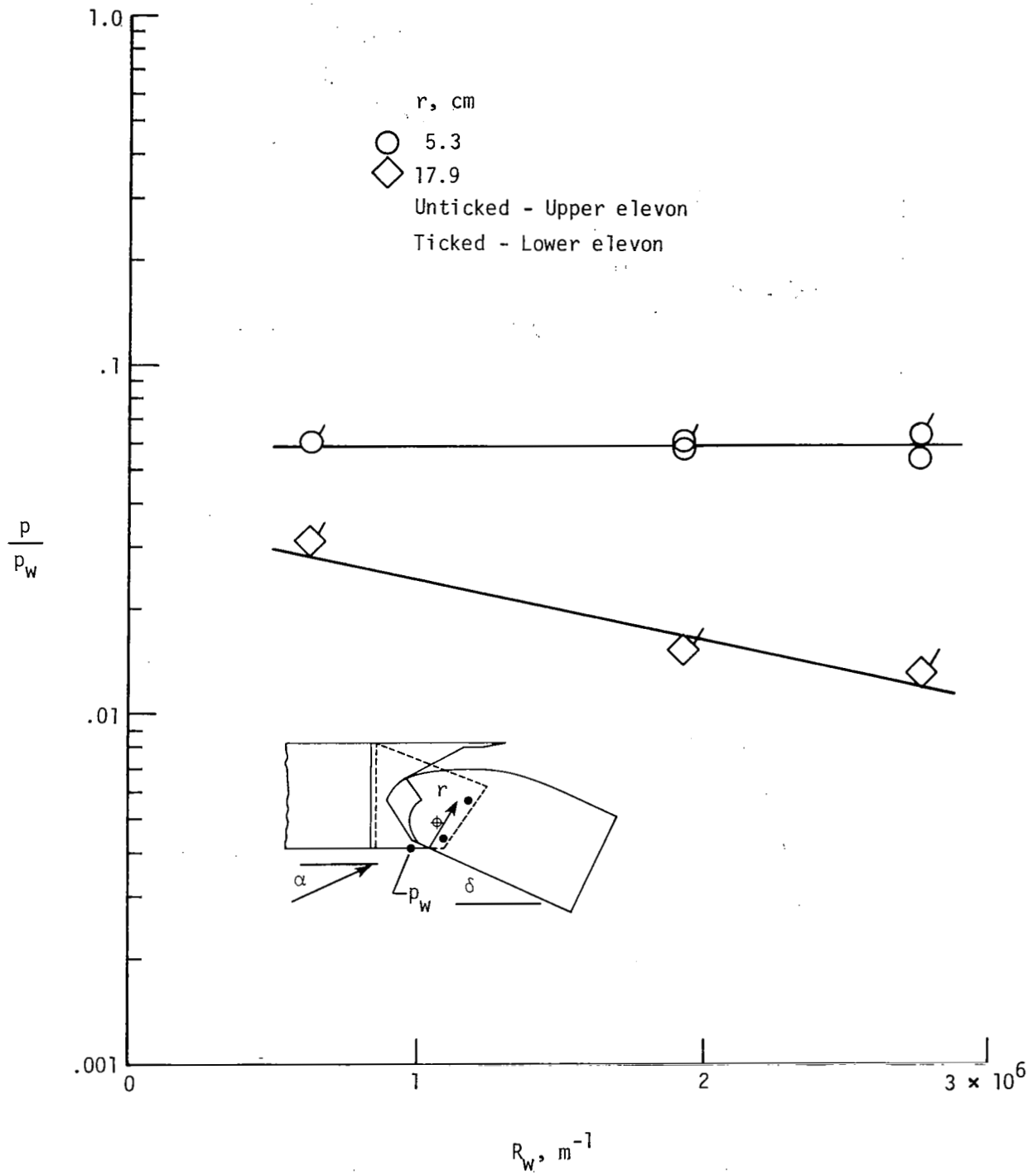

Figure 17.- Variation of elevon-stub gap pressure with local unit Reynolds number. $\alpha = 10^{o}$; $\delta = 10^{o}$; w = 1.19 cm.

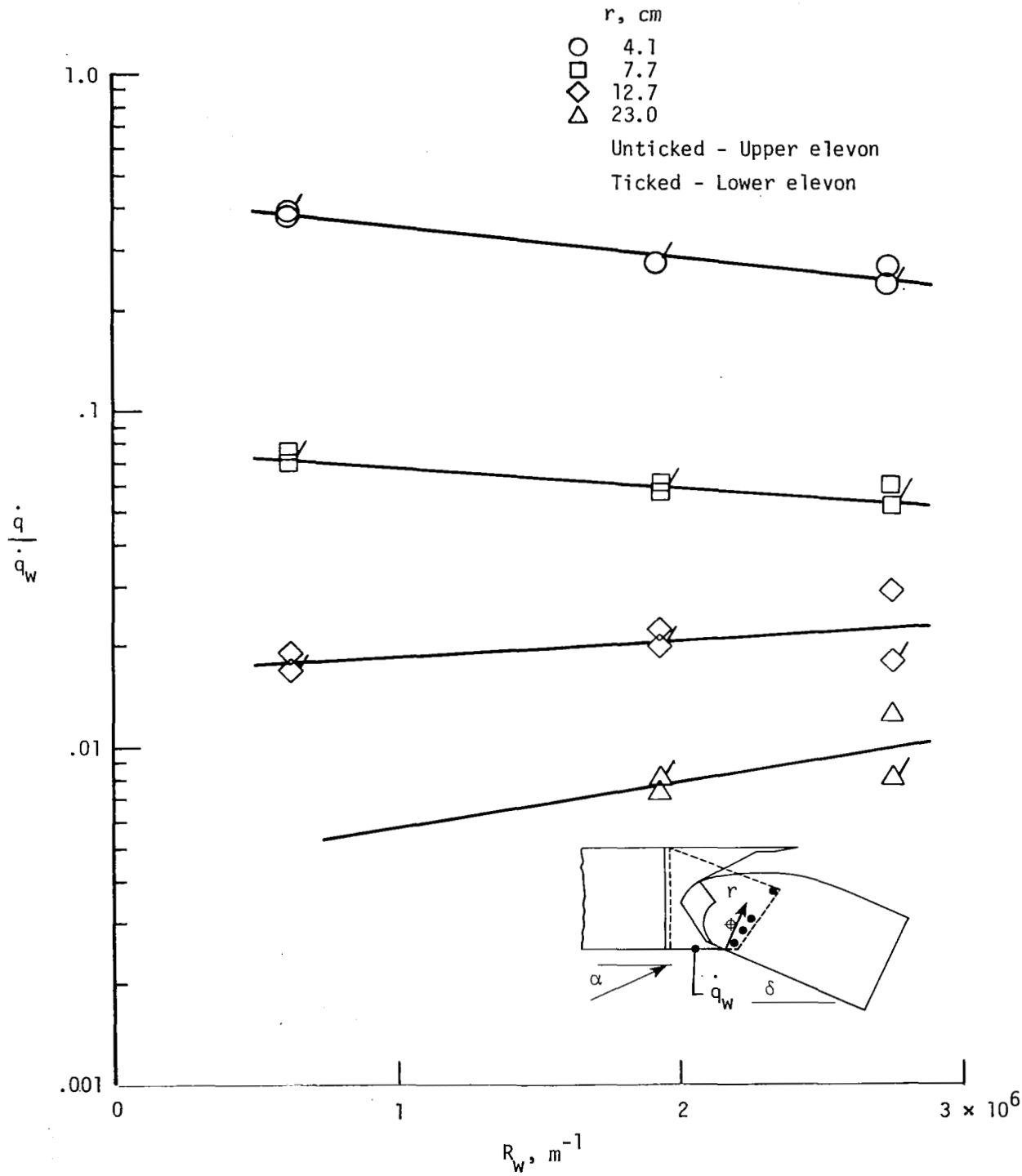

Figure 18.- Variation of elevon-stub gap heating with local unit Reynolds number. $\alpha = 10^{\circ}$; $\delta = 10^{\circ}$; $w = 1.19$ cm.

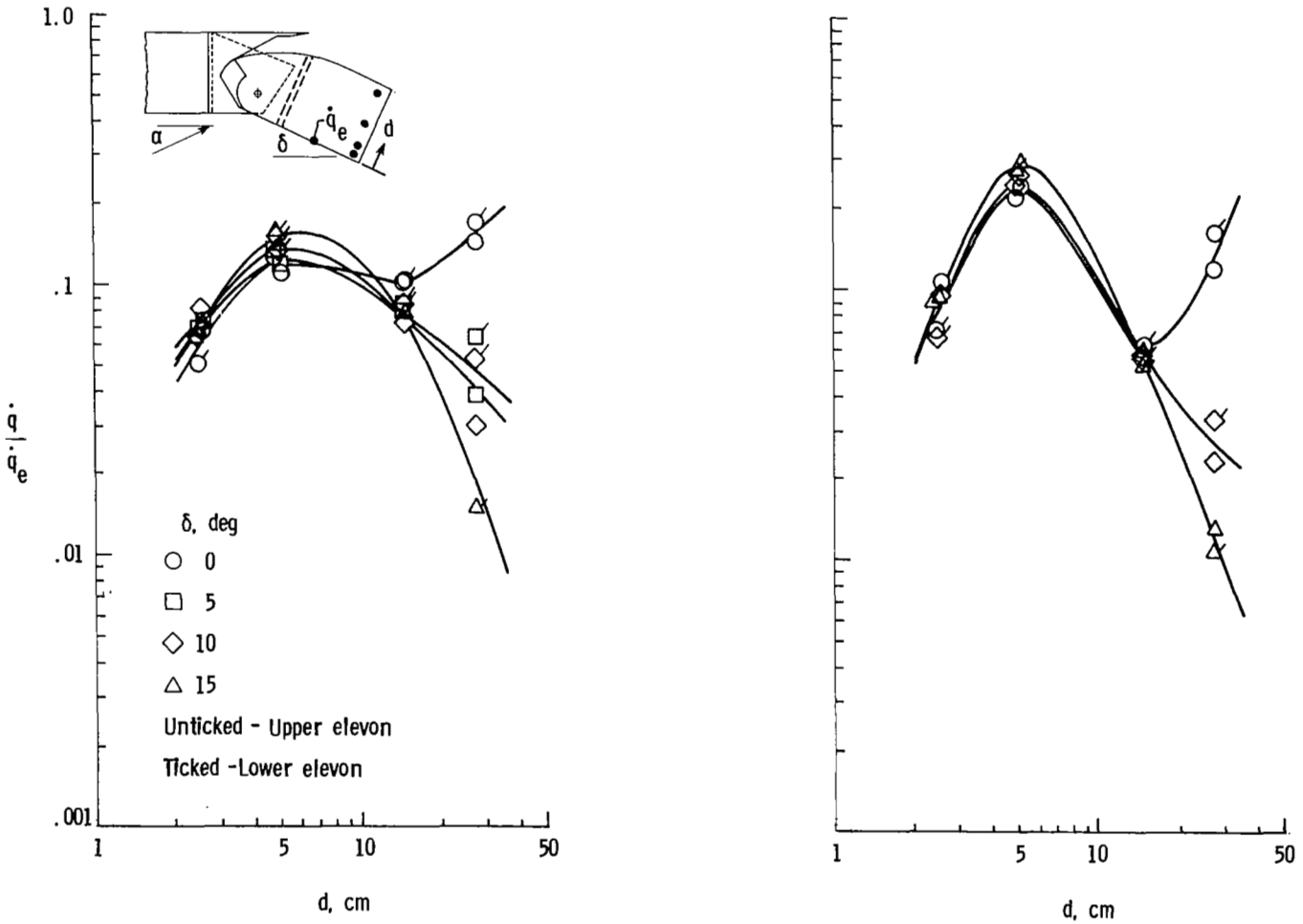

Figure 19.- Elevon gap heating distribution for various elevon deflection angles. $\alpha = 10^{o}$.

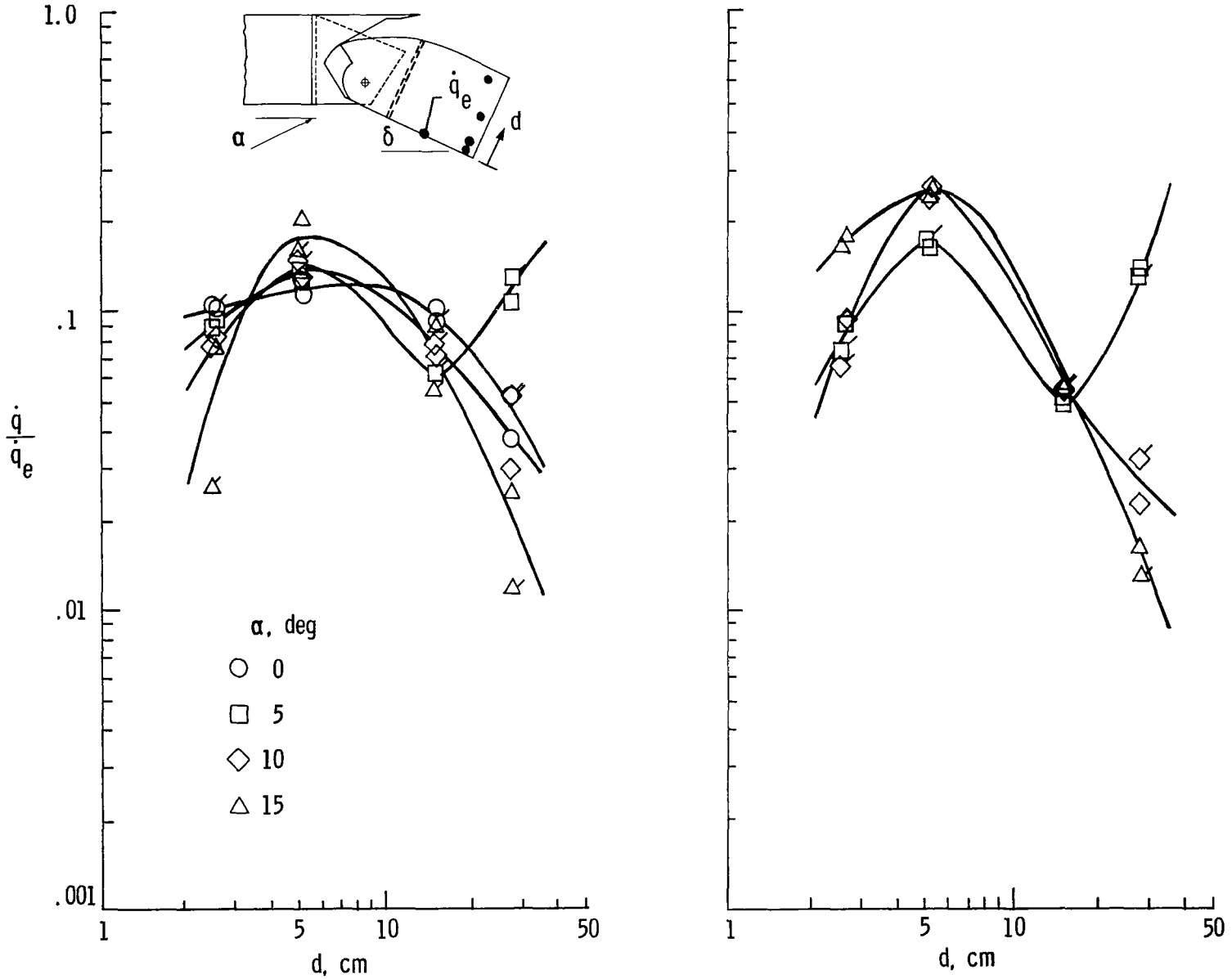

(a) W = 9.65 cm.

(b) W = 8.08 cm.

Figure 20.- Elevon gap heating distribution for various angles of attack. $\delta = 10^{o}$.

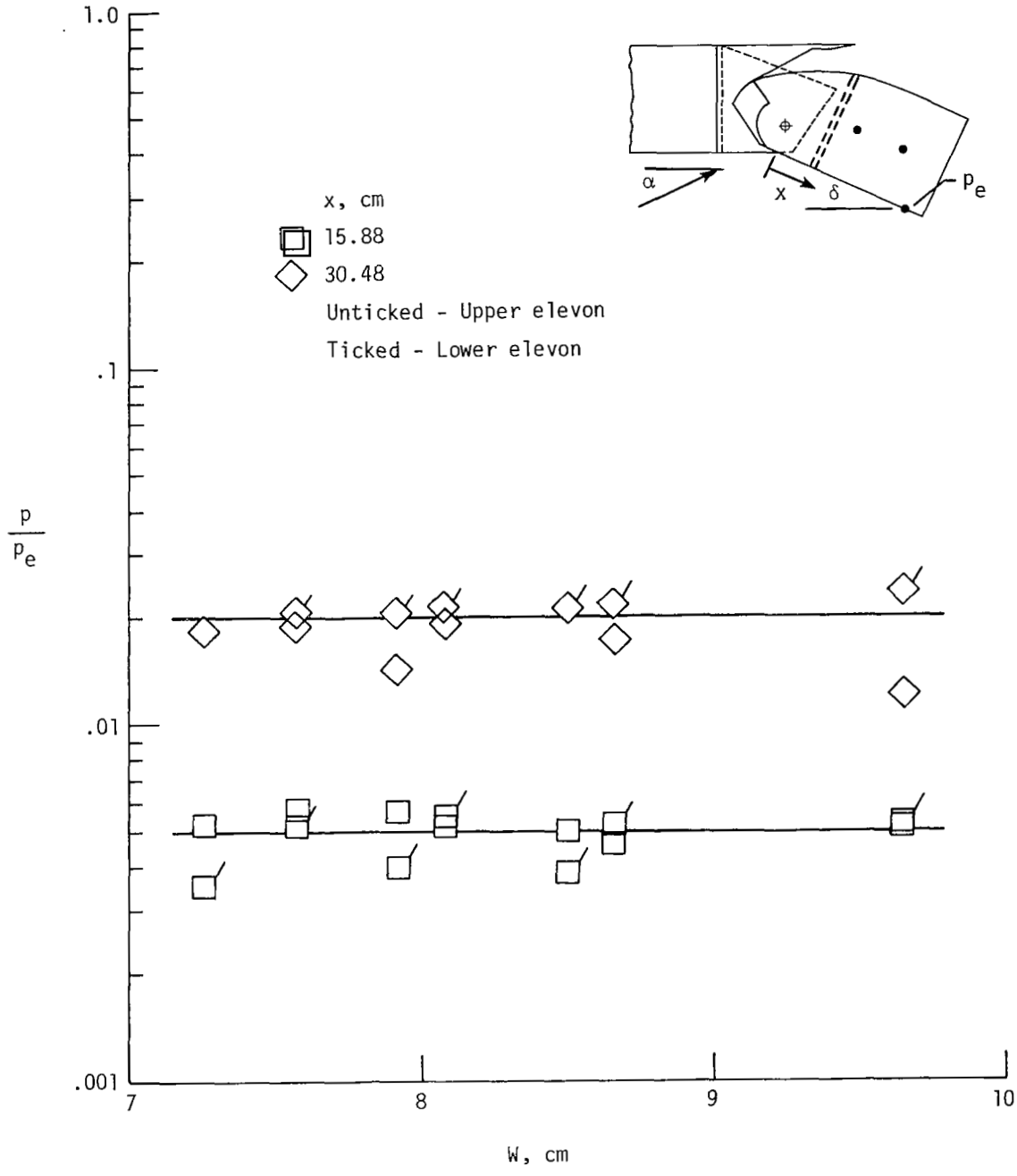

Figure 21.- Variation of elevon gap pressure with gap width. $\alpha = 10^{o}$; $\delta = 10^{o}$; d = 15.2 cm.

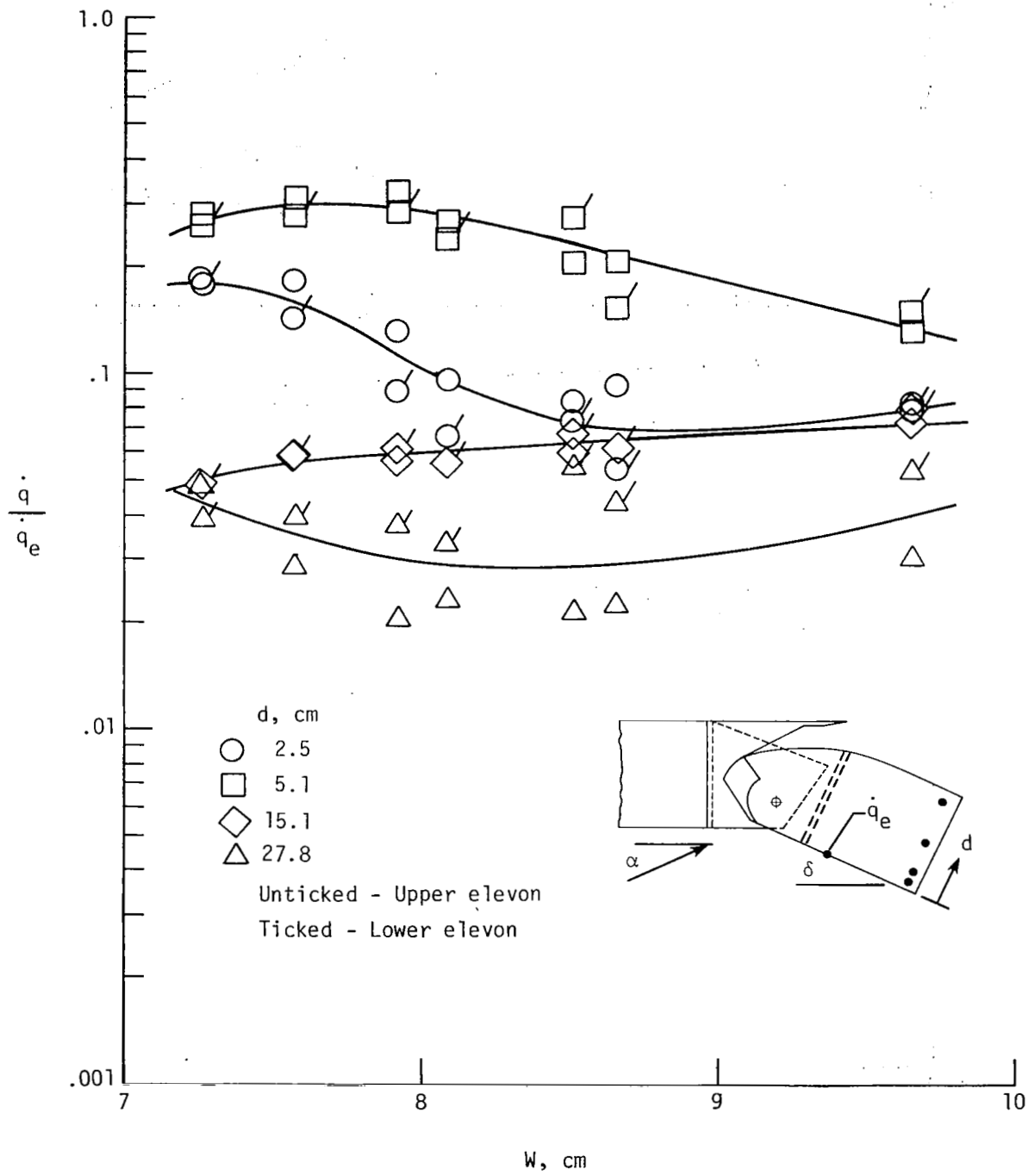

Figure 22.- Variation of elevon gap heating with gap width. $\alpha = 10^{\circ}$; $\delta = 10^{\circ}$.

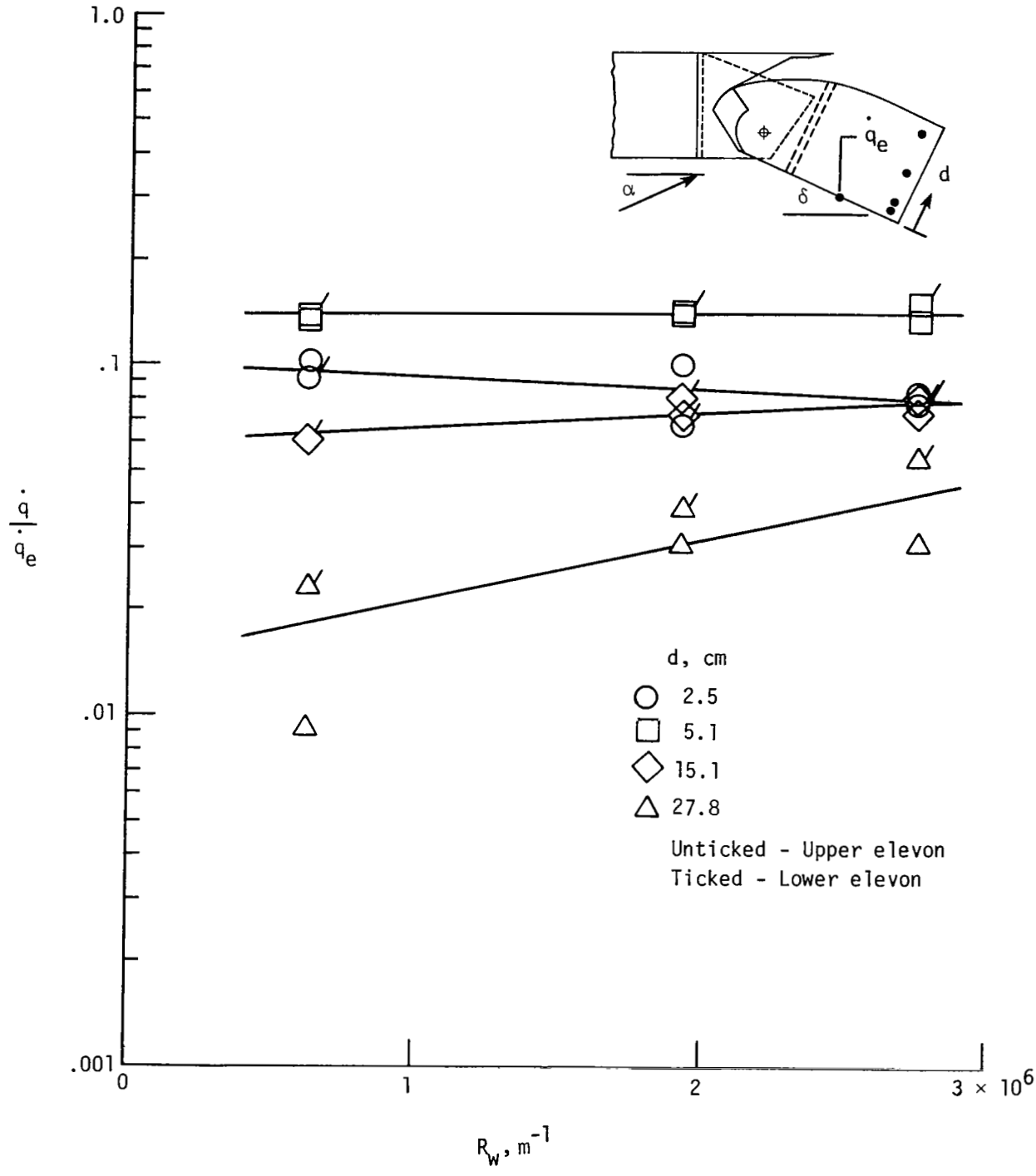

Figure 23.- Variation of elevon gap heating with local unit Reynolds number. $\alpha = 10^{\circ}$; $\delta = 10^{\circ}$; W = 9.65 cm.

1. Report No.	2. Government Accession No.	3. Recipient's Catalog No.
NASA TP-1783		

4. Title and Subtitle	5. Report Date
AEROTHERMAL ENVIRONMENT IN CHORDWISE GAPS BETWEEN SPLIT ELEVONS AT MACH 6.8	December 1980
	6. Performing Organization Code 506-53-53-02

7. Author(s)	8. Performing Organization Report No.
L. Roane Hunt	L-14076
	10. Work Unit No.

9. Performing Organization Name and Address	11. Contract or Grant No.
NASA Langley Research Center Hampton, VA 23665	
	13. Type of Report and Period Covered Technical Paper

12. Sponsoring Agency Name and Address	14. Sponsoring Agency Code
National Aeronautics and Space Administration Washington, DC 20546	

15. Supplementary Notes

16. Abstract

A large-scale model representing a wing-elevon junction on a Shuttle-type entry vehicle was aerothermally tested in the Langley 8-Foot High-Temperature Structures Tunnel with a turbulent boundary layer on the wing and elevon. The flow pattern between elevons was studied, and the pressure and heat load were determined within the chordwise gaps formed by adjacent elevons and by the stub fairing which separates the elevons. Model angle of attack, elevon deflection angle, and gap widths were varied. Heating in the gaps was generally proportional to windward surface heating and inversely proportional to gap width. Maximum heating between the elevon and stub was 36 percent of the windward wing surface for a 0.18-cm-wide elevon-stub gap, and maximum heating between elevons was 30 percent of the heating on the windward elevon surface for a 7.7-cm-wide elevon gap.

17. Key Words (Suggested by Author(s))	18. Distribution Statement
Aerothermal tests Chordwise gaps Split elevons	Unclassified - Unlimited Subject Category 34

19. Security Classif. (of this report)	20. Security Classif. (of this page)	21. No. of Pages	22. Price
Unclassified	Unclassified	42	A03

For sale by the National Technical Information Service, Springfield, Virginia 22161

NASA-Langley, 1980